NCBP2 modulates neurodevelopmental defects of the 3q29 deletion in *Drosophila* and *X. laevis* models

Short title: *Drosophila* and *X. laevis* models of the 3q29 deletion

Mayanglambam Dhruba Singh[1*], Matthew Jensen[1*], Micaela Lasser[2], Emily Huber[1], Tanzeen Yusuff[1], Lucilla Pizzo[1], Brian Lifschutz[1], Inshya Desai[1], Alexis Kubina[1], Sneha Yennawar[1], Sydney Kim[2], Janani Iyer[1], Diego E. Rincon-Limas[3], Laura Anne Lowery[2], and Santhosh Girirajan[1,4]

1. Department of Biochemistry and Molecular Biology, Pennsylvania State University, University Park, PA 16802 USA
2. Department of Biology, Boston College, Chestnut Hill, MA 02467 USA
3. Department of Neurology, McKnight Brain Institute, University of Florida, Gainesville, FL 32611 USA
4. Department of Anthropology, Pennsylvania State University, University Park, PA 16802 USA

*contributed equally to the work

Correspondence:

Santhosh Girirajan, MBBS, PhD
205A Life Sciences Building
Pennsylvania State University
University Park, PA 16802
E-mail: sxg47@psu.edu
Phone: 814-865-0674

ABSTRACT

The 1.6 Mbp deletion on chromosome 3q29 is associated with a range of neurodevelopmental disorders, including schizophrenia, autism, microcephaly, and intellectual disability. Despite its importance towards neurodevelopment, the role of individual genes, genetic interactions, and disrupted biological mechanisms underlying the deletion have not been thoroughly characterized. Here, we used quantitative methods to assay *Drosophila melanogaster* and *Xenopus laevis* models with tissue-specific individual and pairwise knockdown of 14 homologs of genes within the 3q29 region. We identified developmental, cellular, and neuronal phenotypes for multiple homologs of 3q29 genes, potentially due to altered apoptosis and cell cycle mechanisms during development. Using the fly eye, we screened for 314 pairwise knockdowns of homologs of 3q29 genes and identified 44 interactions between pairs of homologs and 34 interactions with other neurodevelopmental genes. Interestingly, *NCBP2* homologs in *Drosophila* (*Cbp20*) and *X. laevis* (*ncbp2*) enhanced the phenotypes of homologs of the other 3q29 genes, leading to significant increases in apoptosis that disrupted cellular organization and brain morphology. These cellular and neuronal defects were rescued with overexpression of the apoptosis inhibitors *Diap1* and *xiap* in both models, suggesting that apoptosis is one of several potential biological mechanisms disrupted by the deletion. *NCBP2* was also highly connected to other 3q29 genes in a human brain-specific interaction network, providing support for the relevance of our results towards the human deletion. Overall, our study suggests that *NCBP2*-mediated genetic interactions within the 3q29 region disrupt apoptosis and cell cycle mechanisms during development.

AUTHOR SUMMARY

Rare copy-number variants, or large deletions and duplications in the genome, are associated with a wide range of neurodevelopmental disorders. The 3q29 deletion confers an increased risk for schizophrenia, autism, and microcephaly. To understand the conserved biological mechanisms that are disrupted by this deletion, we systematically tested 14 individual homologs and 314 pairwise interactions of 3q29 genes for neuronal, cellular, and developmental phenotypes in *Drosophila melanogaster* and *Xenopus laevis* models. We found that multiple homologs of genes within the deletion region contribute towards developmental defects, such as larval lethality and disrupted cellular organization. Interestingly, we found that *NCBP2* acts as a key modifier gene within the region, enhancing the developmental phenotypes of each of the homologs for other 3q29 genes and leading to disruptions in apoptosis and cell cycle pathways. Our results suggest that multiple genes

2

64   within the 3q29 region interact with each other through shared mechanisms and jointly

65   contribute to neurodevelopmental defects.

66

3

INTRODUCTION

Rare copy number variants (CNVs), including deletions and duplications in the human genome, significantly contribute to complex neurodevelopmental disorders such as schizophrenia, intellectual disability/developmental delay, autism, and epilepsy [1,2]. Despite extensive phenotypic heterogeneity associated with recently described CNVs [3], certain rare CNVs have been linked to specific neuropsychiatric diagnoses. For example, the 22q11.2 deletion (DiGeorge/velocardiofacial syndrome), the most frequently occurring pathogenic CNV, is found in about 1-2% of individuals with schizophrenia [4,5], and animal models of several genes within the region show neuronal and behavioral phenotypes on their own [6,7]. Similarly, the 1.6 Mbp recurrent deletion on chromosome 3q29, encompassing 21 genes, was initially identified in individuals with a range of neurodevelopmental features, including intellectual disability, microcephaly, craniofacial features, and speech delay [8,9]. Further studies have implicated this deletion as a major risk factor for multiple disorders [10]. In fact, the deletion confers a >40-fold increase in risk for schizophrenia [11,12] as well as a >20-fold increase in risk for autism [13]. More recently, two studies have reported decreases in body and brain sizes as well as a range of behavioral and social defects in mouse models of the entire deletion, mimicking the human developmental phenotypes associated with the deletion [14,15].

Identifying the biological underpinnings of the 3q29 deletion is contingent upon uncovering the conserved molecular mechanisms linking individual genes or combinations of genes within the 3q29 region to the neurodevelopmental phenotypes observed in individuals with the entire deletion. Recent studies have suggested a subset of genes in the 3q29 region as potential candidates for these phenotypes based on their established roles in neuronal development [16,17]. For example, *DLG1* is a scaffolding protein that organizes the synaptic structure at neuromuscular junctions [18], affecting both synaptic density and plasticity during development [19]. However, mouse models of *Dlg1*$^{+/-}$ did not recapitulate the behavioral and developmental phenotypes observed in mice with the entire deletion [14], suggesting that haploinsufficiency of *DLG1* by itself does not account for the wide range of phenotypes associated with the deletion. Given that genes within rare pathogenic CNV regions tend to share similar biological functions [20] and interact with each other to contribute towards developmental phenotypes [21,22], it is likely that multiple genes within 3q29 jointly contribute to these phenotypes through shared cellular pathways. Therefore, an approach that integrates functional analysis of individual genes within the 3q29 deletion and

4

100   their combinatorial effects on neuronal and cellular phenotypes is necessary to understand the

101   pathways and mechanisms underlying the deletion.

102   Systematic testing of genes within 3q29 towards developmental and cellular

103   phenotypes requires model systems that are amenable for rapid phenotypic evaluation and

104   allow for testing interactions between multiple dosage-imbalanced genes without affecting

105   the viability of the organism. *Drosophila melanogaster* and *Xenopus laevis* provide such

106   powerful genetic models for studying conserved mechanisms that are altered in

107   neurodevelopmental disorders, with the ability to manipulate gene expression in a tissue-

108   specific manner in *Drosophila* [23] and examine developmental defects in *X. laevis* [24].

109   Both model systems contain homologs for a majority of disease-causing genes in humans,

110   and show a high degree of conservation in key developmental pathways [23,25–27]. For

111   example, *Drosophila* knockdown models of the candidate schizophrenia gene *DTNBP1*

112   showed dysregulation of synaptic homeostasis and altered glutamatergic and dopaminergic

113   neuron function [28,29], and fly models for *UBE3A*, the gene associated with Angelman

114   syndrome, showed sleep, memory and locomotor defects [30]. Furthermore, *X. laevis* models

115   have been widely used to identify morphological and neuronal defects associated with

116   developmental disorders [24], such as dendritic connectivity defects with overexpression of

117   *MECP2*, the causative gene for Rett syndrome [31]. Thus, *Drosophila* and *X. laevis* models

118   of individual CNV homologs and their interactions would allow for a deeper dissection of the

119   molecular mechanisms disrupted by the deletion, complementing the phenotypes documented

120   in mouse models of the entire deletion [14,15].

121   Here, we used a mechanistic approach to understand the role of individual homologs

122   of 3q29 genes and their interactions towards the cellular processes underlying the deletion.

123   We systematically characterized developmental, cellular, and nervous system phenotypes for

124   14 conserved homologs of human 3q29 genes and 314 pairwise interactions using

125   *Drosophila,* and validated these phenotypes using *X. laevis*. We found that multiple

126   homologs of genes within the 3q29 region, including *NCBP2, DLG1, FBXO45, PIGZ,* and

127   *BDH1*, contribute to disruptions in apoptosis and cell cycle pathways, leading to neuronal and

128   developmental defects in both model systems. These defects were further enhanced when

129   each of the homologs were concomitantly knocked down with homologs of *NCBP2* in

130   *Drosophila* (*Cbp20*) and *X. laevis* (*ncbp2*), resulting in increased apoptosis and dysregulation

131   of cell cycle genes. Our results support an oligogenic model for the 3q29 deletion, and

132   implicate specific cellular mechanisms disrupted by genes in the deletion region.

RESULTS

Reduced expression of individual homologs of 3q29 genes causes global developmental defects

We used reciprocal BLAST and orthology prediction tools (see Methods) to identify fly homologs for 15 of the 21 genes within the 3q29 deletion region (**Fig. 1, S1 Table**). We note that the genes and crosses tested in this study are represented as fly gene names along with the human counterparts at first mention in the text, i.e. *Cbp20* (*NCBP2*), and fly genes with allele names in the figures, i.e. *Cbp20^{KK109448}*. We found that the biological functions of these 15 genes were also conserved between *Drosophila* and humans, as 61 of the 69 Gene Ontology terms (88.4%) annotations for the human genes were also annotated for their respective fly homologs (**S1 File**). For example, *dlg1* (*DLG1*) and *Cbp20* (*NCBP2*) share the same roles in both flies and vertebrates, as a scaffolding protein at the synaptic junction [32] and a member of the RNA cap binding complex [33], respectively. We used RNA interference (RNAi) and the *UAS-GAL4* system to knockdown expression levels of fly homologs of genes within the 3q29 region ubiquitously and in neuronal, wing and eye tissues [34] (**Fig. 1**). A stock list of the fly lines used in this study and full genotypes for all experiments are provided in **S2 File**. Quantitative PCR (qPCR) confirmed partial knockdown of gene expression for each of the tested homologs (**S2 Table**); fly lines for *CG5359* (*TCTEX1D2*) were excluded from further analysis after additional quality control assessment (see Methods). To identify genes essential for organism survival and neurodevelopment, we first assessed the effect of ubiquitous knockdown of homologs of 3q29 genes using the *da-GAL4* driver (**Fig. 2A**). Seven of the 14 homologs, including *dlg1*, *Cbp20,* and *Tsf2* (*MFI2*), showed lethality or severe developmental defects with ubiquitous knockdown, suggesting that multiple homologs of 3q29 genes are essential for viability during early development. Similarly, wing-specific *bx^{MS1096}-GAL4* knockdown of *Tsf2*, *Cbp20, CG8888* (*BDH1*), and *Pak* (*PAK2*) showed severe wing defects, and wing-specific knockdown of *dlg1* showed larval lethality (**S1 Fig.**).

Several fly homologs for genes within the 3q29 region have previously been associated with a range of neuronal defects during fly development (**S3 Table**). For example, loss of *dlg1* contributed to morphological and physiological defects at the neuromuscular junction (NMJ), as well as increased brain size, abnormal courtship behavior, and loss of gravitaxis response [35–37]. Similarly, *Pak* mutant flies exhibited extensive defects in the axonal targeting of sensory and motor neurons [38,39], in addition to abnormal NMJ and mushroom body development [40,41]. We sought to determine whether fly homologs for

6

167   other genes in the 3q29 region also contribute to defects in neuronal function, and therefore

168   performed climbing assays for motor defects and staining of larval brains for axonal targeting

169   with pan-neuronal knockdown of the fly homologs. Interestingly, *Elav-GAL4* mediated pan-

170   neuronal knockdown caused larval or pupal lethality in *dlg1*, *Tsf2*, and *CG5543* (*WDR53*)

171   flies (**Fig. 2A**), and about 30% of adult flies with knockdown of *dlg1* did not survive beyond

172   day 5 (**S1 Fig.**), indicating an essential role for these genes in neuronal development.

173   Furthermore, we found that flies with pan-neuronal knockdown of several homologs of 3q29

174   genes, including *dlg1* and *Cbp20*, exhibited a strong reduction in climbing ability over ten

175   days (**Fig. 2B, S1 Video**), suggesting that these genes could contribute to abnormalities in

176   synaptic and motor functions [42]. We next examined the axonal projections of photoreceptor

177   cells into the optic lobe by staining third instar larval brains with anti-chaoptin. We found that

178   *GMR-GAL4* mediated eye-specific knockdown of *Cbp20*, *dlg1*, *Pak* and *Fsn* (*FBXO45*)

179   showed several axonal targeting defects (**S1 Fig., S4 Table**). Our results recapitulated the

180   previous findings in *Pak* mutant flies [38], and were similar to targeting defects observed in

181   models of other candidate neurodevelopmental genes, including *Drosophila* homologs for

182   human *DISC1* and *FMR1* [43,44]. Overall, our data show that multiple conserved homologs

183   of genes in the 3q29 region beyond just *dlg1* or *Pak* are important for *Drosophila*

184   neurodevelopment.

185

186   ***Drosophila* eye models for genes within the 3q29 region show cellular defects**

187   The *Drosophila* compound eye has been classically used to perform high-throughput genetic

188   screens and quantitative assays of cellular and neurodevelopmental defects [45]. In fact,

189   about two-thirds of all vital genes in the fly genome are predicted to be involved in fly eye

190   development [46]. For instance, the *Drosophila* eye model was recently used to screen a large

191   set of intellectual disability genes [47], and genetic interaction studies using the fly eye have

192   identified modifier genes for Rett syndrome, spinocerebellar ataxia type 3, and other

193   conserved developmental processes [48–50]. We used the developing fly eye as an *in vivo*

194   system to quantify the effect of gene knockdown on adult eye morphology, cellular

195   organization in the pupal eye, and cell proliferation and death in the larval imaginal eye disc

196   (**Fig. 1**, **S2 Fig.**). The wild-type adult *Drosophila* eye consists of about 750 ommatidia

197   containing different cell types arranged in a regular hexagonal structure, which can be easily

198   perturbed by genetic modifications [51,52]. Because of this, we first performed eye-specific

199   RNAi knockdown of fly homologs of genes in the 3q29 region using *GMR-GAL4*, and

200   measured the rough eye phenotype of each knockdown line using *Flynotyper*, a quantitative

7

201 tool that calculates a phenotypic score based on defects in ommatidial arrangement [53]. We

202 found that eye-specific knockdown of 8/13 homologs of 3q29 genes showed significant

203 external eye phenotypes compared with control *GMR-GAL4* flies, while knockdown of *Tsf2*

204 caused lethality (**Fig. 2C, S3 Fig.**). For example, knockdown of *Cbp20* resulted in a severe

205 rough eye phenotype that was comparable to knockdown of other neurodevelopmental genes

206 [53], such as *Prosap* (*SHANK3*) and *kis* (*CHD8*) (**S5 Table**).

207   To examine the cellular mechanisms underlying the rough eye phenotypes observed

208 with knockdown of fly homologs of 3q29 genes, we first measured changes in area and

209 ommatidial size of the adult eyes. We found a significant reduction in eye size with

210 knockdown of *CG8888* and *Cbp20*, while the eyes of flies with knockdown of *dlg1* were

211 significantly larger than *GMR-GAL4* controls (**Fig. 2D**). Similarly, we observed decreases in

212 ommatidial diameter with knockdown of *Cbp20* and *CG8888*, suggesting that these genes

213 may also contribute to abnormal cell growth phenotypes (**S3 Fig.**). We also assessed the

214 cellular structure of 44 hour-old pupal eyes by staining the ommatidial and photoreceptor

215 cells with anti-DLG, a septate junction marker, and Phalloidin, a marker for F-actin at cell

216 boundaries (**S2 Fig.**). We found that knockdown of 11/12 tested homologs of 3q29 genes

217 caused disorganization or loss of the photoreceptor neurons and ommatidial cells (**Fig. 2E, S4**

218 **Fig., S6 Table**). For example, pupal eyes with knockdown of *CG8888*, *dlg1*, *Cbp20* and

219 *CG5543* all showed defects in cone cell orientation and ommatidial rotation compared with

220 control *GMR-GAL4* flies. Furthermore, *Cbp20* and *dlg1* knockdown flies showed hexagonal

221 defects and severe disorganization of photoreceptor neurons, while *Cbp20* knockdown flies

222 also showed fused secondary cells and *dlg1* knockdown flies showed a complete loss of

223 bristle cells.

224   We next hypothesized that abnormal proliferation and apoptosis could contribute to

225 the cellular defects observed with knockdown of fly homologs of 3q29 genes. To test this, we

226 stained the third instar larval eye discs for select knockdowns of individual homologs of 3q29

227 genes with anti-pH3 (phospho-Histone H3 (Ser10)) and *Drosophila* caspase-1 (dcp1),

228 markers for proliferating and apoptotic cells, and quantified the number of cells posterior to

229 the morphogenetic furrow (**S2 Fig.**). We observed a significant decrease in pH3-positive cells

230 for *CG8888* knockdown flies and trends towards increased pH3-positive cells for *PIG-Z*

231 (*PIGZ*) knockdown flies compared with *GMR-GAL4* controls (p=0.165) (**Fig. 2F, S4 Fig.**),

232 while knockdown of *dlg1* led to significant increases in cells stained with bromodeoxyuridine

233 (BrdU), a marker for replicating cells (**S4 Fig.**). Flies with knockdown of *Cbp20 or dlg1* also

234 showed a significant increase in apoptotic dcp1-positive cells compared with controls (**Fig.**

8

235   **2G**), which we validated using TUNEL assays for these lines (**S4 Fig.**). We further tested for

236   proliferation and apoptosis in the third instar larval wing discs of flies with knockdown of

237   homologs of 3q29 genes using the bx^{MS1096}-*GAL4* driver, and observed changes in both

238   processes with knockdown of *dlg1*, *CG8888* and *Cbp20* (**S5 Fig.**). Knockdown of *Cbp20* in

239   particular showed dcp1-positive staining across the entire wing pouch in the larval wing disc.

240   These data suggest that knockdown of multiple fly homologs of genes in the 3q29 region

241   contribute to defects in apoptosis and proliferation during early development, leading to the

242   observed defects in cell count and organization (**Table 1**).

243

244   **Interactions between fly homologs of 3q29 genes enhance neuronal phenotypes**

245   As knockdown fly models for homologs of multiple 3q29 genes showed a variety of

246   neuronal, developmental, and cellular defects, we hypothesized that these genes could

247   interact with each other to further disrupt cellular processes during development. We

248   therefore generated *GMR-GAL4* recombined lines for nine fly homologs of 3q29 genes, and

249   crossed these lines with multiple RNAi or mutant lines for other homologs to generate 161

250   two-hit crosses for testing 94 pairwise gene interactions (**Fig. 1, S7 Table**). We found a

251   significant enhancement in eye phenotypic severity, measured using *Flynotyper* and validated

252   with a second line when available, for 39 pairwise knockdowns compared with recombined

253   lines crossed with control flies (represented in the figures as $Cbp20^{KK109448}$/*Control*) (**Fig. 3A,**

254   **S6 Fig., S7 Fig.**). In fact, we found that 19 out of 21 pairwise interactions involving *Cbp20* as

255   either a first or second-hit gene resulted in more severe eye phenotypes, suggesting that

256   reduced expression of *Cbp20* drastically modifies the morphological phenotypes of other

257   homologs of 3q29 genes (**Fig. 3B-D**). For further validation, we compared pairs of reciprocal

258   crosses (i.e. *Fsn*/*CG8888* versus *CG8888*/*Fsn*) and confirmed concordant results for 19/26

259   reciprocal interactions, including 14/16 reciprocal interactions involving *Cbp20* (**S7 Table**).

260   We also found a non-significant increase in severity for *dlg1*/*Pak* knockdown flies using both

261   RNAi and mutant lines, concordant with enhanced neuromuscular junction and circadian

262   rhythm defects observed in mutant *dlg1*/*Pak* flies described by Grice and colleagues [54].

263   As *Cbp20* knockdown enhanced the rough eye phenotypes of multiple other

264   homologs, we next tested for enhancement of neuronal defects among flies with knockdown

265   of *Cbp20* and homologs of other 3q29 genes. We found that simultaneous knockdown of

266   *Cbp20* with *dlg1* or *Fsn* led to an increase in severity of axon targeting defects (**Fig. 3E**). For

267   instance, while knockdown of *Cbp20* mostly led to mild-to-moderate axon targeting defects,

268   such as loss of R7-R8 axon projection into the medulla, we observed more severe loss of

9

269   projection for all axons with simultaneous knockdown of *Cbp20* and *dlg1* or *Fsn* (**S4 Table**).

270   We also tested pan-neuronal *Elav-GAL4* knockdown of select pairs of homologs, and found

271   that both *Cbp20/dlg1* and *Cbp20/Fsn* significantly enhanced the climbing defects observed

272   with knockdown of *Cbp20* alone (**Fig. 3F, S2 Video**). Overall, these data show that *Cbp20*

273   interacts with other homologs of genes in the 3q29 region to enhance the observed cellular

274   and neuronal defects (**Table 1**).

275   To further characterize the functional effects of interactions between homologs of

276   3q29 genes, we analyzed changes in gene expression by performing RNA-sequencing of

277   heads from flies with select pan-neuronal knockdown of individual (*Cbp20*, *dlg1*, *Fsn*, and

278   *Pak*) and pairs (*Cbp20/dlg1* and *Cbp20/Fsn*) of homologs of 3q29 genes. We identified

279   differentially-expressed genes in each of the tested fly models compared with *Elav-GAL4*

280   controls, and performed enrichment analysis on both differentially-expressed fly genes and

281   their corresponding human homologs (**S3 File**). We found that knockdown of each individual

282   homolog showed enrichment for dysregulation of cellular and developmental processes (**S8**

283   **Fig.**). For example, flies with knockdown of *dlg1* and *Cbp20* showed enrichment for

284   dysregulation of homologs for human synaptic transmission genes, such as *Glt* (*NLGN1*) and

285   *nAChRβ3* (*HTR3A*). Furthermore, flies with knockdown of *Cbp20* were enriched for

286   dysregulated fly genes related to metabolic processes, while knockdown of *Fsn* led to

287   dysregulation of fly genes involved in response to external stimuli and immune response. We

288   also found that homologs of key signaling genes dysregulated in mouse models of the 3q29

289   deletion, reported by Baba and colleagues [15], were differentially expressed in our fly

290   models for homologs of 3q29 genes. In fact, knockdown of *Fsn* led to altered expression for

291   each of the "early immediate" signaling genes dysregulated in the deletion mouse model [15].

292   While dysregulated genes in *Cbp20/dlg1* knockdown flies showed enrichments for protein

293   folding and sensory perception, *Cbp20/Fsn* knockdown flies were uniquely enriched for

294   dysregulated homologs of cell cycle genes, including *Aura* (*AURKA*), *Cdk1* (*CDK1*), *lok*

295   (*CHEK2*), and *CycE* (*CCNE1*) (**S8 Fig.**). We similarly found 17 differentially-expressed

296   homologs corresponding to human apoptosis genes in *Cbp20/Fsn* knockdown flies, including

297   the DNA fragmentation gene *Sid* (*ENDOG*) and the apoptosis signaling genes *tor* (*RET*) and

298   *Hsp70Bb* (*HSPA1A*). Furthermore, we found a strong enrichment for fly genes whose human

299   homologs are preferentially expressed in early and mid-fetal brain tissues among the

300   dysregulated genes in *Cbp20/Fsn* knockdown flies (**S8 Fig.**). These data suggest that *Cbp20*

301   interacts with other homologs of genes in the 3q29 region to disrupt a variety of key

10

302   biological functions, including apoptosis and cell cycle pathways as well as synaptic

303   transmission and metabolic pathways (**Table 1**).

304   Finally, to complement the interactions among homologs of 3q29 genes that we

305   identified in *Drosophila*, we examined the connectivity patterns of 3q29 genes within the

306   context of human gene interaction databases. Gene interaction networks derived from co-

307   expression and protein-protein interaction data [55,56] showed large modules of connected

308   genes within the 3q29 region, including a strongly-connected component involving 11/21

309   3q29 genes (**Fig. 4A-B**). However, the average connectivity among 3q29 genes within a

310   brain-specific interaction network [57] was not significantly different from the connectivity

311   of randomly-selected sets of genes throughout the genome (**Fig. 4C**), suggesting that a subset

312   of genes drive the complexity of genetic interactions within the region. This paradigm was

313   previously observed among genes in the 22q11.2 deletion region, where interactions between

314   *PRODH* and *COMT* modulate neurotransmitter function independently of other genes in the

315   region [58]. In fact, five genes in the 3q29 region, including *NCBP2*, *PAK2,* and *DLG1*,

316   showed significantly higher connectivity to other 3q29 genes compared with the average

317   connectivity of random sets of genes (**Fig. 4D**). Interestingly, *NCBP2* showed the highest

318   connectivity of all genes in the region, further highlighting its role as a key modulator of

319   genes within the region.

320

321   **Interactions between *Cbp20* and other homologs of 3q29 genes enhance apoptosis**

322   **defects**

323   Cell death and proliferation are two antagonistic forces that maintain an appropriate number

324   of neurons during development [59]. In fact, both processes have been previously identified

325   as candidate mechanisms for several neurodevelopmental disorders [60–62]. While

326   knockdown of *Cbp20* with other homologs of 3q29 genes likely disrupts multiple cellular

327   processes that contribute towards the enhanced cellular defects, we next specifically

328   investigated the role of apoptosis towards these defects, as larval eye and wing discs with

329   knockdown of *Cbp20* showed strong increases in apoptosis. We observed black necrotic

330   patches on the ommatidia in adult eyes with knockdown of *Cbp20/dlg1* and *Cbp20/Fsn*,

331   indicating that an increase in cell death occurs with these interactions (**Fig. 5A, S9 Fig.**). In

332   fact, significantly larger regions of necrotic patches were observed in flies homozygous for

333   *Cbp20* RNAi and heterozygous for *dlg1* RNAi (see **S2 File** for full genotype annotation),

334   suggesting that the knockdown of both homologs contributes to ommatidial cell death (**Fig.**

335   **5A**). Furthermore, we found an enhanced disruption of ommatidial cell organization and loss

11

336   of photoreceptors in pupal flies with concomitant knockdown of *Cbp20* with *dlg1*, *Fsn* or

337   *CG8888*, emphasizing the role of these genes in maintaining cell count and organization (**Fig.**

338   **5B-C, S9 Fig., S8 Table**). Based on these observations, we next assayed for apoptotic cells in

339   the larval eye discs of flies with knockdown of *Cbp20* and other homologs of 3q29 genes. We

340   observed significant increases in the number of apoptotic cells, as measured by dcp1 (**Fig.**

341   **5D-E**) and TUNEL staining (**S9 Fig.**), when *Cbp20* was knocked down along with *CG8888*,

342   *dlg1*, or *Fsn*. *Cbp20/CG8888* knockdown flies also showed a decreased number of pH3-

343   positive cells, suggesting that both apoptosis and proliferation are affected by the interaction

344   between these two genes (**Fig. 5F**).

345   To validate apoptosis as a candidate mechanism for the cellular defects of flies with

346   knockdown of homologs of 3q29 genes, we crossed recombined fly lines for *Cbp20* and *dlg1*

347   with flies overexpressing *Diap1* (death-associated inhibitor of apoptosis). *Diap1* is an E3

348   ubiquitin ligase that targets *Dronc*, the fly homolog of caspase-9, and prevents the subsequent

349   activation of downstream caspases that lead to apoptosis [63]. We found that overexpression

350   of *Diap1* rescued the adult rough eye phenotypes (**Fig. 6A-B, S10 Fig.**) and increased the eye

351   sizes of *Cbp20* and *dlg1* flies (**S10 Fig.**). These observations were corroborated by the

352   reversal of cellular changes in the eye upon *Diap1* overexpression, including the rescue of

353   ommatidial structure and cell count deficits observed with knockdown of *Cbp20* and *dlg1*

354   (**Fig. 6D, S10 Fig.**). Furthermore, overexpression of *Diap1* led to significant reductions in the

355   number of TUNEL and dcp1-positive cells in the larval eye discs of flies with knockdown of

356   *Cbp20* and *dlg1*, confirming the rescue of apoptosis defects in these flies (**Fig. 6E-F**, **S10**

357   **Fig.**). Interestingly, *Diap1* overexpression also suppressed the photoreceptor axon targeting

358   defects observed with knockdown of *Cbp20* (**Fig. 6G, S4 Table**), suggesting that the

359   neuronal defects observed in these flies could be attributed to increased apoptosis. We further

360   confirmed these mechanistic findings by observing increased severity in cellular phenotypes

361   upon overexpression of *Dronc* in *Cbp20* and *dlg1* knockdown flies. For example, we

362   observed black necrotic patches (**Figs. 6A and 6C**) and exaggerated apoptotic responses (**Fig.**

363   **6E-F**, **S10 Fig.**) in *Cbp20* knockdown flies with overexpression of *Dronc*. These results

364   suggest that apoptosis mediates the cellular defects observed in flies with knockdown of

365   *Cbp20* and *dlg1*.

366

Homologs of 3q29 genes interact with canonical neurodevelopmental genes

368   We further explored the role of 3q29 genes in neurodevelopmental pathways by screening

369   four fly homologs with strong neurodevelopmental phenotypes (*Cbp20*, *dlg1*, *CG8888*, and

12

370 *Pak*) for interactions with homologs of 15 known human neurodevelopmental genes, for a

371 total of 60 pairwise interactions and 153 two-hit crosses (**Fig. 7A**). We selected these

372 neurodevelopmental genes for screening based on their association with developmental

373 disorders in humans [53,64], and included eight genes associated with apoptosis or cell cycle

374 functions as well as four genes associated with microcephaly [65], a key phenotype observed

375 in approximately 50% of 3q29 deletion carriers [8]. We found that 34 pairwise interactions,

376 validated with a second line when available, led to significant increases in eye phenotypes

377 compared with recombined lines for individual homologs of 3q29 genes (**S9 Table, S11**

378 **Fig.**). These interactions included 19 validated interactions of homologs of 3q29 genes with

379 apoptosis or cell cycle genes as well as ten interactions with microcephaly genes. We found

380 that 13/15 homologs of neurodevelopmental genes, including all four microcephaly genes,

381 enhanced the phenotypes observed with knockdown of *Cbp20* alone. Furthermore,

382 knockdown of *dlg1* significantly enhanced the ommatidial necrotic patches observed with

383 knockdown of *arm* (*CTNNB1*), while flies with concomitant knockdown of *Cbp20* and *arm*

384 also showed increased necrotic patches (**Fig. 7B, S9 Fig.**). Interestingly, we also found that

385 knockdown of *CG8888* and *dlg1* suppressed the rough eye phenotypes observed with

386 knockdown of *Prosap* (*SHANK3*), while knockdown of *Pak* suppressed the phenotypes of

387 both *Prosap* and *Pten* (*PTEN*) knockdown flies (**Fig. 7B**). Several of these interactions have

388 been previously observed to modulate neuronal function in model systems. For example,

389 *SHANK3* interacts with *DLG1* through the mediator protein DLGAP1 to influence post-

390 synaptic density in mice [66] and binds to proteins in the Rac1 complex, including PAK2, to

391 regulate synaptic structure [67,68]. These results suggest that homologs of 3q29 genes

392 interact with key developmental genes in conserved pathways to modify cellular phenotypes.

393

Reduction of 3q29 gene expression causes developmental defects in *Xenopus laevis*

395 After identifying a wide range of neurodevelopmental defects due to knockdown of fly

396 homologs of 3q29 genes, we sought to gain further insight into the conserved functions of

397 these genes in vertebrate embryonic brain development using the *Xenopus laevis* model

398 system. We examined the effect of targeted knockdown of *ncbp2*, *fbxo45*, and *pak2*, as

399 homologs of these genes displayed multiple severe phenotypes with reduced gene expression

400 in flies. Knockdown of *X. laevis* homologs for each 3q29 gene was accomplished using

401 antisense morpholino oligonucleotides (MOs) targeted to early splice sites of each homolog

402 (**Fig. 1**). *X. laevis* embryos were injected at either the two- or four-cell stage with various

403 concentrations of MO for each homolog or a standard control, and knockdown of each

13

404   homolog was validated using qPCR (**S12 Fig.**). As knockdown of *Cbp20*, *Fsn*, and *Pak* each

405   resulted in neuronal defects in *Drosophila*, we first examined the effects of knockdown of

406   these homologs on *X. laevis* brain development at stage 47. To test this, we knocked down

407   each gene in half of the embryo at the two-cell stage, and left the other half uninjected to

408   create a side-by-side comparison of brain morphology (**Fig. 8A**). We performed whole-mount

409   immunostaining with anti-alpha tubulin and found that reduced expression of *ncbp2*, *fbxo45*,

410   and *pak2* each resulted in smaller forebrain and midbrain size compared with controls (**Fig.**

411   **8A-C**). We also found that simultaneous knockdown of *ncbp2* with *fbxo45* caused a

412   significant decrease in forebrain size and a trend towards decreased midbrain size (p=0.093)

413   compared with *ncbp2* knockdown (**Fig. 8A-C**). Knockdown of *pak2* with *ncbp2* showed a

414   similar trend towards decreased forebrain size (p=0.051). Interestingly, the reduced brain

415   volumes we observed with knockdown of homologs of 3q29 genes in *X. laevis* recapitulate

416   the reduced brain volume observed in 3q29 deletion mice [14,15], suggesting that multiple

417   genes in the 3q29 region contribute to this phenotype. We further examined the effect of

418   knocking down homologs of 3q29 genes on *X. laevis* eye development at stage 42, and found

419   that knockdown of these homologs caused irregular shapes and decreased size compared with

420   controls (**S13 Fig.**). The reductions in eye size were rescued to control levels when mRNA

421   was co-injected along with MO for each homolog (**S13 Fig.**). Together, these data show that

422   individual and pairwise knockdown of homologs of 3q29 genes in *X. laevis* leads to abnormal

423   brain and eye morphology, confirming the conserved role of these genes during vertebrate

424   development.

425   To determine if the knockdown of homologs of 3q29 genes also disrupted apoptotic

426   processes in *X. laevis*, we tested whether overexpression of the X-linked inhibitor of

427   apoptosis gene (*xiap*) could rescue the observed developmental defects. We found that

428   overexpression of *xiap* rescued the midbrain and forebrain size deficits observed with *ncbp2*

429   knockdown to control levels (**Fig. 8A-C**). Similarly, we found that the decreased eye sizes

430   and morphological defects observed with knockdown of *ncbp2* were rescued with *xiap*

431   overexpression (**S13 Fig.**). To further validate these findings, we performed a western blot

432   following knockdown of *fbxo45* and *ncbp2* using anti-cleaved caspase-3 (Asp175) as a

433   marker for apoptosis (**Fig. 8D, S12 Fig.**). We found that reduction of *fbxo45* and *ncbp2*

434   expression each led to an increase in cleaved caspase-3 levels compared with controls, which

435   were restored to control levels with concomitant overexpression of *xiap* (**Fig. 8E**). Caspase-3

436   levels were also enhanced when *fbxo45* and *ncbp2* were knocked down together (**Fig. 8E**),

437   suggesting that these two homologs interact with each other and contribute towards

14

438   developmental phenotypes through increased apoptosis. Overall, these results suggest

439   involvement of apoptotic processes towards the developmental phenotypes observed with

440   knockdown of homologs of 3q29 genes in a vertebrate model (**Table 1**).

441

15

DISCUSSION

Using complementary *Drosophila* and *X. laevis* models, we interrogated developmental effects, cellular mechanisms, and genetic interactions of individual homologs of genes within the 3q29 region. Our major findings were recapitulated across both model systems (**Table 1**) and could also potentially account for the developmental phenotypes reported in mouse models of the entire deletion. Several themes have emerged from our study that exemplify the genetic and mechanistic complexity of the 3q29 deletion region.

First, our analysis of developmental phenotypes with knockdown of homologs for individual 3q29 genes showed that a single gene within the region may not be solely responsible for the effects of the deletion. In fact, we found that knockdown of 12 out of 14 fly homologs showed developmental defects in *Drosophila*, while every fly homolog showed an enhanced rough eye phenotype when knocked down along with at least one other homolog (**Fig. 2**). Although our study is limited to examining conserved cellular phenotypes of homologs of 3q29 genes in *Drosophila* and *X. laevis*, evidence from other model organisms also supports an oligogenic model for the deletion. In fact, knockout mouse models for several 3q29 genes have been reported to exhibit severe developmental phenotypes, including axonal and synaptic defects in $Fbxo45^{-/-}$ and embryonic lethality in $Pak2^{-/-}$ and $Pcyt1a^{-/-}$ knockout mice [69–71] (**S3 Table**). Notably, although $Dlg1^{+/-}$ or $Pak2^{+/-}$ mice showed a range of neuronal phenotypes compared with control mice, they did not recapitulate the major developmental and behavioral features observed in mouse models of the entire deletion [14,15,72], suggesting that the deletion phenotypes are contingent upon haploinsufficiency of multiple genes in the region (**S10 Table**). Furthermore, several 3q29 genes including *PAK2, DLG1, PCYT1A*, and *UBXN7* are under evolutionary constraint in humans, based on gene pathogenicity metrics (**S1 File**). Two genes in the 3q29 region without fly homologs, *CEP19* and *TFRC*, are also under evolutionary constraint in humans, with *TFRC* having been implicated in neural tube defects and embryonic lethality in mouse models [73]. While no common variants associated with neurodevelopmental traits have been observed in the 3q29 region [74], rare variants of varying effects in 9/21 genes have been identified among patients with different developmental disorders [75–77] (**S1 File**). These data, combined with our findings in *Drosophila* and *X. laevis*, implicate multiple genes within the 3q29 region as potential candidates for neurodevelopmental defects.

Second, our screening of 161 crosses between pairs of fly homologs of 3q29 genes identified 44 interactions that showed enhanced rough eye phenotypes, suggesting that complex interactions among genes in the 3q29 region could contribute towards

16

476   developmental defects (**Fig. 9A**). While we only tested a subset of all possible interactions
477   among the non-syntenic homologs of 3q29 genes in *Drosophila*, our results highlight
478   conserved mechanistic relationships between "parts", or the individual genes, towards
479   understanding the effects of the "whole" deletion. For example, knockdown of *Cbp20*
480   enhanced the phenotypes of 11 out of 12 other fly homologs, suggesting that *NCBP2* could be
481   a key modulator of other genes within the region. *NCBP2* encodes a subunit of the nuclear
482   cap-binding complex (CBC), which binds to the 5' end of mRNA and microRNA in the
483   nucleus [78]. Given the role of the CBC in post-transcriptional regulatory mechanisms such
484   as nonsense-mediated decay, alternative splicing and mRNA transport [79,80], it is possible
485   that disruption of this complex could result in changes to a broad set of genes and biological
486   processes. In fact, our analysis of differentially-expressed genes in *Cbp20* knockdown flies
487   showed disruption of synaptic transmission, cellular respiration, and several metabolic
488   pathways. In contrast to other proposed candidate genes in the 3q29 region, *NBCP2* is not
489   predicted to be pathogenic on its own in humans (**S1 File**) and does not have identified
490   deleterious mutations in sequencing studies of neurodevelopmental disease cohorts so far,
491   indicating its potential role as a modifier of the other candidate genes in the region (**Fig. 9B**).
492   Our results also complement previous reports of synergistic interactions among fly homologs
493   of 3q29 genes in the nervous system [54], representing another hallmark of an oligogenic
494   model for the deletion. As these genetic interactions may vary across different species,
495   developmental timepoints, and tissues, the role of these interactions should be more deeply
496   explored using mouse and human cell culture models.

497   *Third,* we identified disruptions to several cellular processes due to both single and
498   pairwise knockdown of homologs in *Drosophila* and *X. laevis* models (**Table 1**). For
499   example, simultaneous knockdown of homologs of *NCBP2* and *FBXO45* in *Drosophila* led to
500   enhanced cellular disorganization (**Fig. 5**) and altered expression of cell cycle and apoptosis
501   genes (**S8 Figure**), as well as enhanced morphological defects and increased caspase-3 levels
502   in *X. laevis* (**Fig. 8**). We further found that overexpression of the apoptosis inhibitors *Diap1*
503   and *xiap* rescued the cellular and neuronal phenotypes observed with knockdown of
504   homologs of 3q29 genes (**Fig. 6**), providing important validations for the potential
505   involvement of apoptosis in the deletion (**Table 1**). We propose that *NCBP2* could modify
506   several cellular and molecular processes that may not be directly related to apoptosis, but
507   could instead lead to a cascade of biological events that ultimately result in apoptosis (**Fig.**
508   **9B**). Apoptosis mechanisms are well-conserved between *Drosophila*, *X. laevis,* and humans,
509   with key genes such as *XIAP* (*Diap1*), *CASP2* (*Dronc*), *CASP3* (*DrICE*), and *CASP7* (*Dcp-1*)

17

510 sharing the same roles in programmed cell death across the three organisms [81–83]. In fact,

511 we found that fly homologs of human genes annotated for apoptosis function in the Gene

512 Ontology database were also enriched for apoptosis function (n=1,063 fly homologs from

513 1,789 human apoptosis genes; p=5.30×10^{-13}, Fisher's Exact test with Benjamini-Hochberg

514 correction). Although we focused on testing apoptosis phenotypes with knockdown of

515 homologs of 3q29 genes, we note that apoptosis is potentially one of many cellular pathways

516 disrupted by the 3q29 deletion (**Fig. 9B**). In fact, our data implicated knockdown of several

517 homologs of 3q29 genes, including *dlg1* and *CG8888* (*BDH1*), towards abnormal cell

518 proliferation during development. Furthermore, several 3q29 genes have been previously

519 associated with apoptosis or cell cycle regulation functions (**S1 File**). For example, *DLG1* is a

520 tumor suppressor gene whose knockdown in *Drosophila* leads to neoplasms in the developing

521 brain and eye disc [84,85], while *PAK2* is a key downstream mediator of the ERK signaling

522 pathway for neuronal extension and is activated by caspases during apoptosis [70,86,87]. Our

523 results recapitulate the role of *DLG1* towards cell cycle regulation, and also implicate *NCBP2*

524 and its interactions towards multiple cellular and developmental phenotypes.

525   More broadly, genes involved with apoptosis and cell proliferation have been

526 implicated in several neurodevelopmental disorders. For example, we previously observed

527 disrupted cell proliferation upon knockdown of *Drosophila* homologs of genes in the 16p11.2

528 deletion region, as well as an enrichment of cell cycle function among connector genes

529 between pairs of 16p11.2 genes in a human brain-specific network [21]. Furthermore,

530 abnormal apoptosis in the early developing brain has been suggested as a possible mechanism

531 for the decreased number of neurons observed in individuals with autism and schizophrenia

532 [62,88,89]. For example, increased apoptosis was observed in both postmortem brain tissue

533 from autism patients [90] and primary fibroblasts from schizophrenia patients [91,92]. We

534 found further support for the role of apoptosis in these disorders by identifying significant

535 enrichments for genes associated with apoptotic processes among candidate genes for autism

536 (empirical p<1.00×10^{-5}) [77], intellectual disability (p<1.00×10^{-5}) [93], and schizophrenia

537 (p=0.014) [76] (**S11 Table**). In fact, out of the 525 neurodevelopmental genes involved in

538 apoptosis, 20 genes were present within pathogenic CNV regions [94], including *CORO1A,*

539 *MAPK3* and *TAOK2* in the 16p11.2 region as well as *TBX1*, the causative gene for heart

540 defects in DiGeorge/velocardiofacial syndrome [95] (**S4 File**). In addition to neuropsychiatric

541 disorders, apoptosis has also been implicated in syndromic forms of microcephaly in humans

542 [96] as well as decreased brain size in animal models of microcephaly genes [97,98]. For

543 example, a mouse model of the Nijmegen breakage syndrome gene *NBN* exhibited increased

18

544   neuronal apoptosis, leading to microcephaly and decreased body mass [99]. Overall, these

545   findings highlight the importance of cell cycle-related processes, particularly apoptosis and

546   proliferation, towards modulating neuronal phenotypes that could be responsible for

547   developmental disorders.

548   In this study, the use of *Drosophila* and *X. laevis* models, both of which are amenable

549   to high-throughput screening of developmental phenotypes, allowed us to systematically

550   examine the conserved cellular and mechanistic roles of homologs of 3q29 genes and their

551   interactions. Follow-up studies in more evolutionarily advanced systems, such as mouse or

552   human cell lines, will be useful to overcome limitations of *Drosophila* and *X. laevis* models,

553   including testing the neurodevelopmental phenotypes and interactions of 3q29 genes without

554   fly homologs. Collectively, these results emphasize the utility of quantitative functional

555   assays for identifying conserved pathways associated with neurodevelopmental disorders,

556   which will hopefully allow for future discoveries of treatments for these disorders.

557

MATERIALS AND METHODS

Fly stocks and genetics

Using reciprocal BLAST searches and orthology predictions from the *DIOPT* v.7.1 database [100], we identified 15 fly homologs for the 21 human genes within the chromosome 3q29 region (**S1 Table**). No fly homologs were present for six genes, including *LRRC33, CEP19, RNF168, SMCO1, TFRC,* and *TM4SF19*. We used a similar strategy to identify homologs for other neurodevelopmental genes tested for interactions in this study. Gene Ontology-Slim (GO-Slim) terms for each human gene and fly homolog were obtained from PantherDB [101] and are provided in **S1 File**. RNAi lines for fly homologs were obtained from the Vienna Drosophila Resource Centre [102] (VDRC), including both KK and GD lines, and the Bloomington *Drosophila* Stock Center (BDSC) (NIH P40OD018537). A list of fly RNAi lines used in this study is provided in **S2 File**. Fly RNAi lines for homologs of 3q29 genes were tested for gene knockdown using quantitative PCR (**S1 Table**). As the available KK line for CG5359 (*TCTEX1D2*) showed a wing phenotype consistent with *tiptop* overexpression due to RNAi insertion at the 5'UTR of the gene [103], which we confirmed using qPCR analysis (**S5 File**), we excluded this gene from our experiments. Microarray data and modENCODE Anatomy RNA-Seq from FlyBase [104,105] showed that all of the 14 tested homologs were expressed in the fly central nervous system and eye tissues (**S1 Table**).

All fly stocks and crosses were cultured on conventional cornmeal-sucrose-dextrose-yeast medium at 25°C, unless otherwise indicated. RNAi lines were crossed with a series of *GAL4* driver lines to achieve tissue-specific knockdown of genes, including w^{1118};*da-GAL4* (Scott Selleck, Penn State) for ubiquitous, w^{1118};*dCad-GFP,GMR-GAL4/CyO* (Zhi-Chun Lai, Penn State) and w^{1118};*GMR-GAL4*;*UAS-Dicer2* (Claire Thomas, Penn State) for eye-specific, w^{1118},*bx^{MS1096}-GAL4;;UAS-Dicer2* (Zhi-Chun Lai, Penn State) for wing-specific, and w^{1118},*Elav-GAL4* (Mike Groteweil, VCU) and w^{1118},*Elav-GAL4;;UAS-Dicer2* (Scott Selleck, Penn State) for pan-neuronal knockdown of gene expression. A list of full genotypes for all crosses tested in this study is provided in **S2 File**. To perform interaction studies, we generated recombined stock lines of *GMR-GAL4* with reduced expression of nine select homologs of 3q29 genes (**S2 File**). Females from these stocks with constitutively reduced gene expression for each of these genes were crossed with RNAi lines of other homologs to achieve simultaneous knockdown of two genes (**Fig. 1**). We previously demonstrated that these two-hit crosses had adequate *GAL4* to bind to two independent *UAS-RNAi* constructs [21].

20

Quantitative polymerase chain reaction for *Drosophila* RNAi knockdowns

Levels of gene expression knockdown were confirmed using quantitative reverse-transcriptase PCR (qPCR) on RNA isolated from pooled groups of 35 fly heads per line tested (**S2 Table**). Briefly, RNAi lines were crossed with *Elav-GAL4* (to test RNAi line efficacy) or *Elav-GAL4;;UAS-Dicer2* (to test for *tiptop* overexpression) at 25°C to achieve pan-neuronal knockdown of the fly homolog. Adult fly heads at day 3 were separated by vortexing, and total RNA was isolated using TRIzol (Invitrogen, Carlsbad, CA, USA). cDNA was prepared using the qScript cDNA synthesis kit (Quantabio, Beverly, MA, USA). Quantitative PCR was performed using an Applied Biosystems Fast 7500 system with SYBR Green PCR master mix (Quantabio) to estimate the level of gene expression. All experiments were performed using three biological replicates of 35 fly heads each. Primers were designed using NCBI Primer-BLAST [106], with primer pairs separated by an intron in the corresponding genomic DNA. A list of primers used in the experiments is provided in **S2 Table**. The delta-delta Ct value method was used to obtain the relative expression of fly homologs in the RNAi lines compared with *Elav-GAL4* controls [107].

Climbing assay

We set up fly crosses at 25°C with *Elav-GAL4* to obtain pan-neuronal knockdown for select homologs of 3q29 genes. For each RNAi line tested, groups of ten female flies were first allowed to adjust at room temperature for 30 minutes and then transferred to a climbing apparatus, made by joining two vials, and allowed to adjust for 5 minutes. The flies were tapped down to the bottom, and the number of flies climbing past the 8 cm mark measured from the bottom of the apparatus in 10 seconds was then counted (**S1 Video, S2 Video**). This assay was repeated nine additional times for each group, with a one-minute rest between trials. The sets of 10 trials for each group were repeated daily for ten days, capturing data for 100 replicates from day 1 until day 10, starting the experiments with 1-2-day old flies. All experiments were performed during the same time of the day for consistency of results.

Imaging of adult fly eyes and wings

We crossed RNAi lines with *GMR-GAL4* and reared at 29°C for eye-specific knockdown and *bx^MS1096^-GAL4* at 25°C for wing-specific knockdown. For eye imaging, adult 2-3-day old female progenies from the crosses were collected, immobilized by freezing at -80°C, mounted on Blu-tac (Bostik Inc, Wauwatosa, WI, USA), and imaged with an Olympus BX53 compound microscope with LMPLan N 20X air objective using a DP73 c-mount camera at

21

626   0.5X magnification and a z-step size of 12.1μm. (Olympus Corporation, Tokyo, Japan). We

627   used CellSens Dimension software (Olympus Corporation, Tokyo, Japan) to capture the

628   images, and stacked the image slices using Zerene Stacker (Zerene Systems LLC, Richland,

629   WA, USA). All eye images presented in this study are maximum projections of 20

630   consecutive optical z-sections. Adult wings were plucked from 2-5 day old female flies,

631   mounted on a glass slide, covered with a coverslip and sealed with clear nail polish. The

632   wings were imaged using a Zeiss Discovery V20 stereoscope (Zeiss, Thornwood, NY, USA)

633   with ProgRes Speed XT Core 3 camera (Jenoptik AG, Jena, Germany) using a 40X objective,

634   and wing images were captured with ProgRes CapturePro v.2.8.8.

635

Quantitative phenotyping of fly eyes using *Flynotyper*

637   We used a computational method called *Flynotyper* (https://flynotyper.sourceforge.net) to

638   measure the degree of roughness of the adult eyes with knockdown of individual or pairs of

639   homologs [53]. The software uses an algorithm to detect the center of each ommatidium, and

640   calculates a phenotypic score based on the number of ommatidia detected, the lengths of six

641   local vectors with direction pointing from each ommatidium to the neighboring ommatidia,

642   and the angle between these six local vectors (**S2 Fig.**). Eye areas, ommatidial diameter, and

643   areas of necrotic patches, which may not be reflected in the *Flynotyper* scores, were

644   measured using ImageJ [108]. Significant pairwise interactions were reported as "validated"

645   when multiple RNAi or mutant lines, if available, showed the same phenotype (**S7 Table, S9**

646   **Table**).

647

Immunohistochemistry of eye and wing discs

649   Third instar larval and 44-hour-old pupal eye discs, reared at 29°C, and third instar larval

650   wing discs, reared at 25°C, were dissected in 1X phosphate-buffered saline (PBS) and fixed

651   in 4% paraformaldehyde for 20 minutes. The eye and wing discs were then washed thrice in

652   PBT (PBS with 0.1% Triton-X) for 10 minutes each, treated with blocking solution (PBS

653   with 1% normal goat serum (NGS) for eye discs, or 1% bovine serum albumin (BSA) for

654   wing discs) for 30 minutes, and then incubated overnight with primary antibodies at 4°C.

655   Rabbit anti-cleaved *Drosophila* dcp1 (Asp216) (1:100; 9578S, Cell Signaling Technology,

656   Danvers, MA, USA), a marker for cells undergoing apoptosis, and Mouse anti-phospho-

657   Histone H3 (S10) antibody (1:100; 9706L, Cell Signaling Technology), a mitotic marker for

658   measuring proliferating cells, were used to assay cell proliferation and apoptosis defects in

659   larval eye and wing discs. Mouse anti-DLG (1:200; 4F3, DSHB, Iowa City, Iowa, USA), a

660   septate junction marker, and Rhodamine Phalloidin (1:200; R415, Invitrogen Molecular

661   Probes, Carlsbad, CA, USA), an F-actin marker, were used to visualize and count ommatidial

662   cells and photoreceptor cells in pupal eyes. Mouse anti-chaoptin (1:200; 24B10, DSHB) was

663   used to visualize retinal axon projections. Preparations were then washed thrice with PBT for

664   10 minutes, and incubated for two hours with fluorophore-conjugated secondary antibodies

665   (Alexa fluor 568 goat anti-mouse (1:200) (A11031), Alexa fluor 488 goat anti-mouse (1:200)

666   (A11029), Alexa fluor 647 goat anti-rabbit (1:200) (A21245), and Alexa fluor 647 goat anti-

667   mouse (1:200) (A21236), Invitrogen Molecular Probes, Carlsbad, CA, USA)) with gentle

668   shaking. Preparations were washed thrice in PBT for 10 minutes, and the tissues were then

669   mounted in Prolong Gold antifade mounting media with DAPI (P36930, Thermo Fisher

670   Scientific, Waltham, MA, USA) or Vectashield hard set mounting media with DAPI (H-

671   1500, Vector Laboratories, Burlingame, CA, USA) for imaging.

672

673   **Bromouridine staining**

674   Third instar larval eye discs were dissected in 1X PBS and immediately transferred to

675   Schneider's Insect Media (Sigma-Aldrich, St. Louis, MO). The tissues were then incubated in

676   10 μM BrdU (Sigma-Aldrich) at 25°C for one hour with constant agitation to allow for

677   incorporation of BrdU into DNA of replicating cells during the S-phase of cell cycle. The

678   samples were washed thrice with PBS for five minutes each and fixed in 4%

679   paraformaldehyde for 20 minutes. To denature DNA, the tissues were acid-treated in 2N HCl

680   for 20 minutes, neutralized in 100 mM Borax solution for 2 minutes, washed thrice in 10X

681   PBT (PBS with 0.1% Tween-20) for 10 minutes, and treated with blocking solution (PBS,

682   0.2% Triton X-100, 5% NGS) for one hour. The tissues were then incubated in mouse anti-

683   BrdU (1:200; G3G4, DSHB, Iowa City, Iowa, USA) and diluted in blocking solution

684   overnight at 4°C. The next day, the tissues were washed thrice in PBT for 20 minutes each

685   and incubated in Alexa fluor 568 goat anti-mouse (1:200, Invitrogen Molecular Probes,

686   Carlsbad, CA, USA) for two hours with constant agitation. Finally, the samples were

687   mounted in Prolong Gold antifade reagent with DAPI (Thermo Fisher Scientific, Waltham,

688   MA, USA) for imaging.

689

690   **Terminal deoxynucleotidyl transferase (TUNEL) Assay**

691   The levels of cell death in the developing eye were evaluated by staining using the *In Situ*

692   Cell Death Detection Kit, TMR Red (Roche, Basel, Switzerland). The third instar larval eye

693   discs were dissected in 1X PBS and fixed in 4% paraformaldehyde for 20 minutes at room

694   temperature, followed by three 10-minute washes with PBS. The dissected tissues were

695   permeabilized by treating with 20 µg/ml proteinase K (Sigma-Aldrich, St. Louis, MO, USA)

696   for two minutes, washed thrice in PBT (PBS with 0.1% Triton-X) for 5 minutes each, fixed in

697   4% paraformaldehyde for 15 minutes, and washed thrice again in PBT for 10 minutes each.

698   The tissues were then incubated overnight with TUNEL (terminal deoxynucleotidyl

699   transferase dUTP nick end labeling) reaction mixture at 4°C per the manufacturer's

700   instructions, and washed five times in PBT for 15 minutes each. Finally, tissues were

701   mounted in Prolong-gold antifade containing DAPI (Thermo Fisher Scientific, Waltham,

702   MA, USA) for imaging.

703

704   **Confocal imaging and analysis**

705   Confocal images of larval and pupal eye discs were captured using an Olympus Fluoview

706   FV1000 laser scanning confocal microscope (Olympus America, Lake Success,

707   NY). Maximum projections of all optical sections were generated for display. As DLG

708   staining was only used to visualize cell boundaries in the pupal eye and not for any

709   expression or quantitative analysis, we increased the laser intensity from 400-490V in

710   control flies to 530-570V in flies with knockdown of *dlg1* to account for decreased DLG

711   expression. Acquisition and processing of images was performed using the Fluoview

712   FV10-ASW 2.1 software (Olympus Corporation, Tokyo, Japan), and the z-stacks of images

713   were merged using ImageJ [108]. The number of pH3, BrdU, TUNEL, and dcp1-positive

714   cells from larval eye discs were counted using two ImageJ plugins, AnalyzeParticles and

715   Image-based Tool for Counting Nuclei (ITCN). As we found a strong correlation (Pearson

716   correlation, $r=0.736$, $p<2.2 \times 10^{-16}$) between the two methods (**S2 Fig.**), all cell counts

717   displayed for eye data were derived from ITCN analysis. Proliferating cells in larval wing

718   discs stained with pH3 were counted using AnalyzeParticles, and apoptotic cells in wing

719   discs stained with dcp1 were analyzed using manual counting. Images stained with anti-

720   chaoptin were manually scored as having either "mild" (minor axon disorganization

721   compared with control), "moderate" (partial loss of axon projection. i.e. loss of R7-R8

722   projection into the medulla), or "severe" (loss of projections for most axons at the lamina)

723   axon targeting defects.

724

725   **Differential expression analysis of transcriptome data**

726   We performed RNA sequencing (RNA-Seq) of samples isolated from three biological

727   replicates of 35 fly heads each for individual (*Cbp20*, *dlg1*, *Fsn*, *Pak*) and pairwise

24

728 (*Cbp20/dlg1*, *Cbp20/Fsn*) *Elav-GAL4* mediated knockdowns of homologs of 3q29 genes. We

729 compared gene expression levels of each cross to VDRC control flies carrying the same

730 genetic background (GD or KK control lines crossed with *Elav-GAL4*). We prepared cDNA

731 libraries for the three biological replicates per genotype using TruSeq Stranded mRNA LT

732 Sample Prep Kit (Illumina, San Diego, CA), and performed single-end sequencing using

733 Illumina HiSeq 2000 at the Penn State Genomics Core Facility to obtain 100 bp reads at an

734 average coverage of 36.0 million aligned reads/sample. We used Trimmomatic v.0.36 [109]

735 for quality control assessment, TopHat2 v.2.1.1 [110] to align the raw sequencing data to the

736 reference fly genome and transcriptome (build 6.08), and HTSeq-Count v.0.6.1 [111] to

737 calculate raw read counts for each gene. edgeR v.3.20.1 [112] (generalized linear model

738 option) was used to perform differential expression analysis, and genes with $\log_2$-fold

739 changes >1 or <-1 and false-discovery rates <0.05 (Benjamini-Hochberg correction) were

740 considered to be differentially expressed (**S3 File**). Human homologs of differentially-

741 expressed fly genes (top matches for each fly gene, excluding matches with "low" rank) were

742 identified using DIOPT [100]. Enrichment analysis of Panther GO-Slim Biological Process

743 terms among the differentially-expressed fly genes and their human homologs was performed

744 using the PantherDB Gene List Analysis tool [101]. Enrichments for genes preferentially

745 expressed in the developing brain were calculated using the Cell-type Specific Expression

746 Analysis tool [113] based on expression data from the BrainSpan Atlas [114].

747

748 *X. laevis* **embryos**

749 Eggs collected from female *X. laevis* frogs were fertilized *in vitro*, dejellied, and cultured

750 following standard methods [115,116]. Embryos were staged according to Nieuwkoop and

751 Faber [117]. All *X. laevis* experiments were approved by the Boston College Institutional

752 Animal Care and Use Committee (Protocol #2016-012) and were performed according to

753 national regulatory standards.

754

755 **Morpholino and RNA constructs**

756 Morpholinos (MOs) were targeted to early splice sites of *X. laevis ncbp2*, *fbxo45*, *pak2*, or

757 standard control MO, purchased from Gene Tools LLC (Philomath, OR, USA). MO

758 sequences are listed in **S12 Table**. For knockdown experiments, all MOs were injected at

759 either the 2-cell or 4-cell stage, with embryos receiving injections two or four times total in

760 0.1X MMR media containing 5% Ficoll. Control and *fbxo45* MOs were injected at

761 10ng/embryo, *ncbp2* and control MOs were injected at 20ng/embryo, and *pak2* and control

25

762   MOs were injected at 50ng/embryo. For rescue experiments (**S13 Fig.**), the same amounts of

763   MOs used in the KD experiments were injected along with gene-specific mRNA tagged with

764   GFP (800pg/embryo for *xiap*-GFP; 1000pg/embryo for *ncbp2*-GFP and *fbxo45*-GFP, and

765   300pg/embryo for *pak2*-GFP) in the same injection solution. Capped mRNAs were

766   transcribed *in vitro* using SP6 or T7 mMessage mMachine Kit (Thermo Fisher Scientific,

767   Waltham, MA, USA). RNA was purified with LiCl precipitation. *X. laevis ncbp2*, *fbxo45*,

768   *pak2*, and *xiap* ORFs obtained from the European *Xenopus* Resource Center (EXRC,

769   Portsmouth, UK) were gateway-cloned into pCSf107mT-GATEWAY-3'GFP destination

770   vectors. Constructs used included *ncbp2*-GFP, *fbxo45*-GFP, *pak2*-GFP, *xiap*-GFP, and GFP

771   in pCS2+. Embryos either at the 2-cell or 4-cell stage received four injections in 0.1X MMR

772   containing 5% Ficoll with the following total mRNA amount per embryo: 300pg of GFP,

773   800pg of *xiap*-GFP, 1000pg of *ncbp2*-GFP, 1000pg of *fbxo45*-GFP, and 300pg of *pak2*-GFP.

774

775   **qPCR for *X. laevis* morpholino knockdown**

776   Morpholino validation and knockdown was assessed using qPCR. Total RNA was extracted

777   using TRIzol reagent (Life Technologies, Grand Island, NY, USA), followed by chloroform

778   extraction and ethanol precipitation from 2-day old embryos injected with increasing

779   concentrations of MO targeted to each homolog of the tested 3q29 gene. cDNA synthesis was

780   performed with SuperScript II Reverse Transcriptase (Life Technologies, Grand Island, NY,

781   USA) and random hexamers. PCR primers are listed in **S13 Table**. qPCR was performed in

782   triplicate (**S12 Fig.**), with band intensities quantified by densitometry in ImageJ and

783   normalized to the uninjected control mean relative to *ODC1*, which was used as a

784   housekeeping control.

785

786   **Brain and eye morphology assays**

787   In brain morphology experiments, all embryos received two injections at the 2-cell stage in

788   0.1X MMR containing 5% Ficoll. One cell was left uninjected and the other cell was injected

789   with either control MO or MO targeted to the tested 3q29 gene, along with 300pg of GFP

790   mRNA in the same injection solution. Stage 47 tadpoles were fixed in 4% PFA diluted in

791   PBS for one hour, rinsed in PBS and gutted to reduce autofluorescence. Embryos were

792   incubated in 3% bovine serum albumin and 1% Triton-X 100 in PBS for two hours, and then

793   incubated in anti-acetylated tubulin primary antibody (1:500, monoclonal, clone 6-11B-1,

794   AB24610, Abcam, Cambridge, UK) and goat anti-mouse Alexa fluor 488 conjugate

795   secondary antibody (1:1000, polyclonal, A11029, Invitrogen Life Technologies, Carlsbad,

26

796 CA). Embryos were then rinsed in 1% PBS-Tween and imaged in PBS. Skin dorsal to the

797 brain was removed if the brain was not clearly visible due to pigment. For eye phenotype

798 experiments, all embryos received four injections at the 2-cell or 4-cell stage in 0.1X MMR

799 containing 5% Ficoll with either the control MO or MOs targeted to each 3q29 gene. Stage

800 42 tadpoles were fixed in 4% PFA diluted in PBS. Tadpoles were washed three times in 1%

801 PBS-Tween for one hour at room temperature before imaging.

802

803 *X. laevis* **image acquisition and analysis**

804 Lateral view images of stage 42 tadpoles for eye experiments and dorsal view images of state

805 47 tadpoles for brain experiments were each collected on a SteREO Discovery.V8

806 microscope using a Zeiss 5X objective and Axiocam 512 color camera (Zeiss, Thornwood,

807 NY, USA). Areas of the left and right eye, forebrain, and midbrain were determined from raw

808 images using the polygon area function in ImageJ. Eye size was quantified by taking the

809 average area of both the left and right eye, while forebrain and midbrain area were quantified

810 by taking the ratio between the injected and uninjected sides for each sample.

811

812 **Western blot for apoptosis**

813 Two replicate western blot experiments were performed to test for apoptosis markers in *X.*

814 *laevis* with 3q29 gene knockdown (**S12 Figure**). Embryos at stages 20-22 were lysed in

815 buffer (50mM Tris pH 7.5, 1% NP40, 150mM NaCl, 1mM PMSF, 0.5 mM EDTA)

816 supplemented with cOmplete Mini EDTA-free Protease Inhibitor Cocktail (Sigma-Aldrich,

817 Basel, Switzerland). Blotting was carried out using rabbit polyclonal antibody to cleaved

818 caspase-3 (1:500, 9661S, Cell Signaling Technology, Danvers, MA, USA), with mouse anti-

819 beta actin (1:2500, AB8224, Abcam, Cambridge, UK) as a loading control on a Mini-

820 PROTEAN TGX precast 4-15% gradient gel (Bio-Rad, Hercules, CA, USA).

821 Chemiluminescence detection was performed using Amersham ECL western blot reagent

822 (GE Healthcare Bio-Sciences, Pittsburgh, PA, USA). Band intensities were quantified by

823 densitometry in ImageJ and normalized to the control mean relative to beta-actin. Due to the

824 low number of replicates, we did not perform any statistical tests on data derived from these

825 experiments.

826

827 **Human brain-specific network analysis of 3q29 gene interactions**

828 We used a human brain-specific gene interaction network that was previously built using a

829 Bayesian classifier trained on gene co-expression datasets [56,57]. We extracted interactions

830   between pairs of genes with predicted weights >2.0 (containing the top 0.5% most likely

831   interactions) and measured the length of the shortest paths connecting pairs of 3q29 genes

832   within the network, excluding genes without connectivity in the network from final

833   calculations. As a control, we also measured the connectivity of 500 randomly selected genes

834   with 100 replicates each of 20 other random genes. All network analysis was performed using

835   the NetworkX Python package [118].

836

837   **Overlap between neurodevelopmental and apoptosis gene sets**

838   We obtained a set of 1,794 genes annotated with the Gene Ontology term for apoptotic

839   processes (GO:0006915) or children terms from the Gene Ontology Consortium (AmiGO

840   v.2.4.26) [119], and overlapped this gene set with sets of 756 candidate autism genes (SFARI

841   Gene Tiers 1-4) [77], 1,854 candidate intellectual disability genes [93], and 2,546 curated

842   candidate schizophrenia genes [76]. Genes in these three sets that were annotated for

843   apoptosis function are listed in **S4 File**. To determine the statistical significance of these

844   overlaps, we performed 100,000 simulations to identify the number of apoptosis genes among

845   groups of genes randomly selected from the genome, and determined the percentiles for each

846   observed overlap among the simulated overlaps as empirical p-values.

847

848   **Statistical analysis**

849   Details of each dataset and the associated statistical tests are provided in **S5 File**. All

850   statistical analyses of functional data were performed using R v.3.4.2 (R Foundation for

851   Statistical Computing, Vienna, Austria). Non-parametric one-tailed and two-tailed Mann-

852   Whitney tests were used to analyze *Drosophila* functional data and human network data, as

853   several datasets were not normally distributed ($p < 0.05$, Shapiro-Wilk tests for normality).

854   Climbing ability and survival data for each fly RNAi line across each experiment day were

855   analyzed using two-way and one-way repeated values ANOVA tests with post-hoc pairwise

856   t-tests. We also used parametric t-tests to analyze *Drosophila* qPCR data and all *X. laevis*

857   data, as these data were either normally distributed ($p > 0.05$, Shapiro-Wilk tests for normality)

858   or had a robust sample size ($n > 30$) for non-normality. All p-values from statistical tests

859   derived from similar sets of experiments (i.e. *Flynotyper* scores for pairwise interactions,

860   dcp1 rescue experiments with *Diap1*) were corrected using Benjamini-Hochberg correction.

861

862

863

Reproducibility

Drosophila eye area and pH3 and TUNEL staining experiments for select individual knockdown lines, as well as climbing ability experiments for a subset of individual and pairwise knockdown lines, were performed on two independent occasions with similar sample sizes. Data displayed in the main figures were derived from single batches, while data from the repeated experiments are shown in **S14 Fig**. *X. laevis* brain and eye area experiments were performed on three independent occasions, with the data shown in the figures representing pooled results of each of the three experimental batches (normalized to the respective controls from each batch). *X. laevis* qPCR experiments were performed three times and western blot experiments were performed twice, with the blots/gels for each replicate experiment shown in **S12 Fig**. Sample sizes for each experiment were determined by testing all available organisms; no prior power calculations for sample size estimation were performed. No data points or outliers were excluded from the experiments presented in the manuscript.

Data availability

Gene expression data for the six *Drosophila* individual and pairwise RNAi knockdown of homologs of 3q29 genes are deposited in the GEO (Gene Expression Omnibus) database with accession code GSE128094, and the raw RNA Sequencing files are deposited in the SRA (Sequence Read Archive) with BioProject accession PRJNA526450. All other data generated and analyzed in study are included in the manuscript and supporting files. All unique biological materials described in the manuscript, such as recombined fly stocks, are readily available from the authors upon request.

Code availability

All source code and datasets for generating genomic data (RNA-Seq, network analysis, and neurodevelopment/apoptosis gene overlap) are available on the Girirajan lab GitHub page at https://github.com/girirajanlab/3q29_project.

REFERENCES

1.   Malhotra D, Sebat J. CNVs: Harbingers of a rare variant revolution in psychiatric genetics. Cell. 2012;148: 1223–1241. doi:10.1016/j.cell.2012.02.039

2.   Girirajan S, Campbell CD, Eichler EE. Human Copy Number Variation and Complex Genetic Disease. Annu Rev Genet. 2011;45: 203–226. doi:10.1146/annurev-genet-102209-163544

3.   Girirajan S, Eichler EE. Phenotypic variability and genetic susceptibility to genomic disorders. Hum Mol Genet. 2010;19: R176-87. doi:10.1093/hmg/ddq366

4.   Karayiorgou M, Morris MA, Morrow B, Shprintzen RJ, Goldberg R, Borrow J, et al. Schizophrenia susceptibility associated with interstitial deletions of chromosome 22q11. Proc Natl Acad Sci U S A. 1995;92: 7612–7616. doi:10.1073/pnas.92.17.7612

5.   Karayiorgou M, Simon TJ, Gogos JA. 22q11.2 microdeletions: Linking DNA structural variation to brain dysfunction and schizophrenia. Nat Rev Neurosci. 2010;11: 402–416. doi:10.1038/nrn2841

6.   Fenelon K, Mukai J, Xu B, Hsu P-K, Drew LJ, Karayiorgou M, et al. Deficiency of Dgcr8, a gene disrupted by the 22q11.2 microdeletion, results in altered short-term plasticity in the prefrontal cortex. Proc Natl Acad Sci U S A. 2011;108: 4447–4452. doi:10.1073/pnas.1101219108

7.   Mukai J, Tamura M, Fénelon K, Rosen AM, Spellman TJ, Kang R, et al. Molecular substrates of altered axonal growth and brain connectivity in a mouse model of schizophrenia. Neuron. 2015;86: 680–95. doi:10.1016/j.neuron.2015.04.003

8.   Ballif BC, Theisen A, Coppinger J, Gowans GC, Hersh JH, Madan-Khetarpal S, et al. Expanding the clinical phenotype of the 3q29 microdeletion syndrome and characterization of the reciprocal microduplication. Mol Cytogenet. 2008;1: 8. doi:10.1186/1755-8166-1-8

9.   Mulle JG, Dodd AF, McGrath JA, Wolyniec PS, Mitchell AA, Shetty AC, et al. Microdeletions of 3q29 confer high risk for schizophrenia. Am J Hum Genet. 2010;87: 229–236. doi:10.1016/j.ajhg.2010.07.013

10. Glassford MR, Rosenfeld JA, Freedman AA, Zwick ME, Mulle JG. Novel features of 3q29 deletion syndrome: Results from the 3q29 registry. Am J Med Genet Part A. 2016;170: 999–1006. doi:10.1002/ajmg.a.37537

11. Kirov G, Pocklington AJ, Holmans P, Ivanov D, Ikeda M, Ruderfer D, et al. De novo CNV analysis implicates specific abnormalities of postsynaptic signalling complexes in the pathogenesis of schizophrenia. Mol Psychiatry. 2012;17: 142–153. doi:10.1038/mp.2011.154

12. Mulle JG. The 3q29 deletion confers >40-fold increase in risk for schizophrenia. Mol Psychiatry. 2015;20: 1028–1029. doi:10.1038/mp.2015.76

13. Pollak RM, Murphy MM, Epstein MP, Zwick ME, Klaiman C, Saulnier CA, et al. Neuropsychiatric phenotypes and a distinct constellation of ASD features in 3q29 deletion syndrome: results from the 3q29 registry. Mol Autism. 2019;10: 30. doi:10.1186/s13229-019-0281-5

14. Rutkowski TP, Purcell RH, Pollak RM, Grewenow SM, Gafford GM, Malone T, et al. Behavioral changes and growth deficits in a CRISPR engineered mouse model of the schizophrenia-associated 3q29 deletion. Mol Psychiatry. 2019. doi:10.1038/s41380-019-0413-5

15. Baba M, Yokoyama K, Seiriki K, Naka Y, Matsumura K, Kondo M, et al. Psychiatric-disorder-related behavioral phenotypes and cortical hyperactivity in a mouse model of 3q29 deletion syndrome. Neuropsychopharmacology. 2019;44: 2125–2135. doi:10.1038/s41386-019-0441-5

16. Quintero-Rivera F, Sharifi-Hannauer P, Martinez-Agosto JA. Autistic and psychiatric findings associated with the 3q29 microdeletion syndrome: Case report and review. Am J Med Genet Part A. 2010;152 A: 2459–2467. doi:10.1002/ajmg.a.33573

17. Rutkowski TP, Schroeder JP, Gafford GM, Warren ST, Weinshenker D, Caspary T, et al. Unraveling the genetic architecture of copy number variants associated with schizophrenia and other neuropsychiatric disorders. J Neurosci Res. 2017;95: 1144–1160. doi:10.1002/jnr.23970

18. Budnik V, Koh YH, Guan B, Hartmann B, Hough C, Woods D, et al. Regulation of synapse structure and function by the Drosophila tumor suppressor gene dlg. Neuron. 1996;17: 627–640. doi:10.1016/S0896-6273(00)80196-8

19. Walch L. Emerging role of the scaffolding protein Dlg1 in vesicle trafficking. Traffic. 2013;14: 964–973. doi:10.1111/tra.12089

20. Andrews T, Meader S, Vulto-van Silfhout A, Taylor A, Steinberg J, Hehir-Kwa J, et al. Gene Networks Underlying Convergent and Pleiotropic Phenotypes in a Large and Systematically-Phenotyped Cohort with Heterogeneous Developmental Disorders. PLoS Genet. 2015;11: e1005012. doi:10.1371/journal.pgen.1005012

21. Iyer J, Singh MD, Jensen M, Patel P, Pizzo L, Huber E, et al. Pervasive genetic interactions modulate neurodevelopmental defects of the autism-associated 16p11.2 deletion in Drosophila melanogaster. Nat Commun. 2018;9: 2548. doi:10.1038/s41467-018-04882-6

22. Jensen M, Girirajan S. An interaction-based model for neuropsychiatric features of copy-number variants. PLoS Genet. 2019;15: e1007879. doi:10.1371/journal.pgen.1007879

23. Wangler MF, Yamamoto S, Bellen HJ. Fruit flies in biomedical research. Genetics. 2015;199: 639–653. doi:10.1534/genetics.114.171785

24. Pratt KG, Khakhalin AS. Modeling human neurodevelopmental disorders in the Xenopus tadpole: from mechanisms to therapeutic targets. Dis Model Mech. 2013;6: 1057–1065. doi:10.1242/dmm.012138

25. Reiter LT, Potocki L, Chien S, Gribskov M, Bier E. A systematic analysis of human disease-associated gene sequences in Drosophila melanogaster. Genome Res. 2001;11: 1114–1125. doi:10.1101/gr.169101

26. Gatto CL, Broadie K. Drosophila modeling of heritable neurodevelopmental disorders. Curr Opin Neurobiol. 2011;21: 834–841. doi:10.1016/j.conb.2011.04.009

27. Harland RM, Grainger RM. Xenopus research: Metamorphosed by genetics and genomics. Trends Genet. 2011;27: 507–515. doi:10.1016/j.tig.2011.08.003

28. Dickman DK, Davis GW. The schizophrenia susceptibility gene dysbindin controls synaptic homeostasis. Science). 2009;326: 1127–1130. doi:10.1126/science.1179685

29. Shao L, Shuai Y, Wang J, Feng S, Lu B, Li Z, et al. Schizophrenia susceptibility gene dysbindin regulates glutamatergic and dopaminergic functions via distinctive mechanisms in Drosophila. Proc Natl Acad Sci U S A. 2011;108: 18831–18836. doi:10.1073/pnas.1114569108

30. Wu Y, Bolduc F V., Bell K, Tully T, Fang Y, Sehgal A, et al. A Drosophila model for Angelman syndrome. Proc Natl Acad Sci U S A. 2008;105: 12399–12404. doi:10.1073/pnas.0805291105

31. Marshak S, Meynard MM, de Vries YA, Kidane AH, Cohen-Cory S. Cell-autonomous alterations in dendritic arbor morphology and connectivity induced by overexpression of MeCP2 in Xenopus central neurons in vivo. PLoS One. 2012;7: e33153. doi:10.1371/journal.pone.0033153

32. Muller BM, Kistner U, Veh RW, Cases-Langhoff C, Becker B, Gundelfinger ED, et al. Molecular characterization and spatial distribution of SAP97, a novel presynaptic protein homologous to SAP90 and the Drosophila discs-large tumor suppressor protein. J Neurosci. 1995;15: 2354–2366. doi:10.1523/jneurosci.15-03-02354.1995

33. Sabin LR, Zhou R, Gruber JJ, Lukinova N, Bambina S, Berman A, et al. Ars2 Regulates Both miRNA- and siRNA- Dependent Silencing and Suppresses RNA Virus Infection in Drosophila. Cell. 2009;138: 340–351. doi:10.1016/j.cell.2009.04.045

34. Brand AH, Perrimon N. Targeted gene expression as a means of altering cell fates and generating dominant phenotypes. Development. 1993;118: 401–415.

35. Thomas U, Kim E, Kuhlendahl S, Koh YH, Gundelfinger ED, Sheng M, et al. Synaptic clustering of the cell adhesion molecule Fasciclin II by discs- large and its role in the regulation of presynaptic structure. Neuron. 1997;19: 787–799. doi:10.1016/S0896-6273(00)80961-7

36. Armstrong JD, Texada MJ, Munjaal R, Baker DA, Beckingham KM. Gravitaxis in Drosophila melanogaster: A forward genetic screen. Genes, Brain Behav. 2006;5: 222–239. doi:10.1111/j.1601-183X.2005.00154.x

37. Mendoza-Topaz C, Urra F, Barría R, Albornoz V, Ugalde D, Thomas U, et al. DLGS97/SAP97 is developmentally upregulated and is required for complex adult behaviors and synapse morphology and function. J Neurosci. 2008;28: 304–314. doi:10.1523/JNEUROSCI.4395-07.2008

38. Hing H, Xiao J, Harden N, Lim L, Lawrence Zipursky S. Pak functions downstream of Dock to regulate photoreceptor axon guidance in Drosophila. Cell. 1999;97: 853–863. doi:10.1016/S0092-8674(00)80798-9

39. Kim MD, Kamiyama D, Kolodziej P, Hing H, Chiba A. Isolation of Rho GTPase effector pathways during axon development. Dev Biol. 2003;262: 282–293. doi:10.1016/S0012-1606(03)00393-2

40. Parnas D, Haghighi AP, Fetter RD, Kim SW, Goodman CS. Regulation of postsynaptic structure and protein localization by the Rho-type guanine nucleotide exchange factor dPix. Neuron. 2001;32: 415–424. doi:10.1016/S0896-6273(01)00485-8

41. Ng J, Luo L. Rho GTPases regulate axon growth through convergent and divergent signaling pathways. Neuron. 2004;44: 779–793. doi:10.1016/j.neuron.2004.11.014

42. Sherwood NT, Sun Q, Xue M, Zhang B, Zinn K. Drosophila spastin regulates synaptic microtubule networks and is required for normal motor function. PLoS Biol. 2004;2: e429. doi:10.1371/journal.pbio.0020429

43. Chen SY, Huang PH, Cheng HJ. Disrupted-in-schizophrenia 1-mediated axon guidance involves TRIO-RAC-PAK small GTPase pathway signaling. Proc Natl Acad Sci U S A. 2011;108: 5861–5866. doi:10.1073/pnas.1018128108

44. Morales J, Hiesinger PR, Schroeder AJ, Kume K, Verstreken P, Jackson FR, et al. Drosophila fragile X protein DFXR regulates neuronal morphology and function in the brain. Neuron. 2002;34: 961–972. doi:10.1016/S0896-6273(02)00731-6

45. Thomas BJ, Wassarman DA. A fly's eye view of biology. Trends Genet. 1999;15: 184–190. doi:10.1016/S0168-9525(99)01720-5

46. Thaker HM, Kankel DR. Mosaic analysis gives an estimate of the extent of genomic involvement in the development of the visual system in Drosophila melanogaster. Genetics. 1992;131: 883–894.

47. Oortveld MAW, Keerthikumar S, Oti M, Nijhof B, Fernandes AC, Kochinke K, et al. Human Intellectual Disability Genes Form Conserved Functional Modules in Drosophila. PLoS Genet. 2013;9: e1003911. doi:10.1371/journal.pgen.1003911

48. Cukier HN, Perez AM, Collins AL, Zhou Z, Zoghbi HY, Botas J. Genetic modifiers of MeCP2 function in Drosophila. PLoS Genet. 2008;4: e1000179. doi:10.1371/journal.pgen.1000179

49. Bilen J, Bonini NM. Genome-wide screen for modifiers of ataxin-3 neurodegeneration in Drosophila. PLoS Genet. 2007;3: 1950–64. doi:10.1371/journal.pgen.0030177

50. Neufeld TP, Tang AH, Rubin GM. A genetic screen to identify components of the sina signaling pathway in Drosophila eye development. Genetics. 1998;148: 277–286.

51. Cagan RL, Ready DF. The emergence of order in the Drosophila pupal retina. Dev Biol. 1989;136: 346–362. doi:10.1016/0012-1606(89)90261-3

52. Kumar JP. Building an ommatidium one cell at a time. Dev Dyn. 2012;241: 136–149. doi:10.1002/dvdy.23707

53. Iyer J, Wang Q, Le T, Pizzo L, Grönke S, Ambegaokar SS, et al. Quantitative assessment of eye phenotypes for functional genetic studies using Drosophila melanogaster. G3 Genes, Genomes, Genet. 2016;6: 1427–1437. doi:10.1534/g3.116.027060

54. Grice SJ, Liu J-L, Webber C. Synergistic Interactions between Drosophila Orthologues of Genes Spanned by De Novo Human CNVs Support Multiple-Hit Models of Autism.

1060   PLOS Genet. 2015;11: e1004998. doi:10.1371/journal.pgen.1004998

1061   55.   Warde-Farley D, Donaldson SL, Comes O, Zuberi K, Badrawi R, Chao P, et al. The
1062   GeneMANIA prediction server: Biological network integration for gene prioritization
1063   and predicting gene function. Nucleic Acids Res. 2010;38: W214-20.
1064   doi:10.1093/nar/gkq537

1065   56.   Greene CS, Krishnan A, Wong AK, Ricciotti E, Zelaya RA, Himmelstein DS, et al.
1066   Understanding multicellular function and disease with human tissue-specific networks.
1067   Nat Genet. 2015;47: 569–576. doi:10.1038/ng.3259

1068   57.   Krishnan A, Zhang R, Yao V, Theesfeld CL, Wong AK, Tadych A, et al. Genome-
1069   wide prediction and functional characterization of the genetic basis of autism spectrum
1070   disorder. Nat Neurosci. 2016;19: 1454–1462. doi:10.1038/nn.4353

1071   58.   Paterlini M, Zakharenko SS, Lai WS, Qin J, Zhang H, Mukai J, et al. Transcriptional
1072   and behavioral interaction between 22q11.2 orthologs modulates schizophrenia-related
1073   phenotypes in mice. Nat Neurosci. 2005;8: 1586–1594. doi:10.1038/nn1562

1074   59.   Yamaguchi Y, Miura M. Programmed Cell Death in Neurodevelopment. Dev Cell.
1075   2015;32: 478–490. doi:10.1016/j.devcel.2015.01.019

1076   60.   Ernst C. Proliferation and Differentiation Deficits are a Major Convergence Point for
1077   Neurodevelopmental Disorders. Trends Neurosci. 2016;39: 290–299.
1078   doi:10.1016/j.tins.2016.03.001

1079   61.   Pinto D, Pagnamenta AT, Klei L, Anney R, Merico D, Regan R, et al. Functional
1080   impact of global rare copy number variation in autism spectrum disorders. Nature.
1081   2010;466: 368–372. doi:10.1038/nature09146

1082   62.   Glantz LA, Gilmore JH, Lieberman JA, Jarskog LF. Apoptotic mechanisms and the
1083   synaptic pathology of schizophrenia. Schizophr Res. 2006;81: 47–63.
1084   doi:10.1016/j.schres.2005.08.014

1085   63.   Steller H. Regulation of apoptosis in Drosophila. Cell Death Differ. 2008;15: 1132–
1086   1138. doi:10.1038/cdd.2008.50

1087   64.   Coe BP, Girirajan S, Eichler EE. A genetic model for neurodevelopmental disease.
1088   Curr Opin Neurobiol. 2012;22: 829–836. doi:10.1016/j.conb.2012.04.007

1089   65.   Nicholas AK, Swanson EA, Cox JJ, Karbani G, Malik S, Springell K, et al. The
1090   molecular landscape of ASPM mutations in primary microcephaly. J Med Genet.
1091   2009;46: 249–253. doi:10.1136/jmg.2008.062380

1092   66.   Coba MP, Ramaker MJ, Ho E V, Thompson SL, Komiyama NH, Grant SGN, et al.
1093   Dlgap1 knockout mice exhibit alterations of the postsynaptic density and selective
1094   reductions in sociability. Sci Rep. 2018;8: 2281. doi:10.1038/s41598-018-20610-y

1095   67.   Duffney LJ, Zhong P, Wei J, Matas E, Cheng J, Qin L, et al. Autism-like Deficits in
1096   Shank3-Deficient Mice Are Rescued by Targeting Actin Regulators. Cell Rep.
1097   2015;11: 1400–1413. doi:10.1016/j.celrep.2015.04.064

1098   68.   Park E, Na M, Choi J, Kim S, Lee J-R, Yoon J, et al. The Shank Family of
1099   Postsynaptic Density Proteins Interacts with and Promotes Synaptic Accumulation of

1100   the βPIX Guanine Nucleotide Exchange Factor for Rac1 and Cdc42. J Biol Chem.
1101   2003;278: 19220–19229. doi:10.1074/jbc.M301052200

1102   69.   Saiga T, Fukuda T, Matsumoto M, Tada H, Okano HJ, Okano H, et al. Fbxo45 Forms
1103   a Novel Ubiquitin Ligase Complex and Is Required for Neuronal Development. Mol
1104   Cell Biol. 2009;29: 3529–3543. doi:10.1128/mcb.00364-09

1105   70.   Marlin JW, Chang YWE, Ober M, Handy A, Xu W, Jakobi R. Functional PAK-2
1106   knockout and replacement with a caspase cleavage-deficient mutant in mice reveals
1107   differential requirements of full-length PAK-2 and caspase-activated PAK-2p34.
1108   Mamm Genome. 2011;22: 306–317. doi:10.1007/s00335-011-9326-6

1109   71.   Wang L, Magdaleno S, Tabas I, Jackowski S. Early Embryonic Lethality in Mice with
1110   Targeted Deletion of the CTP:Phosphocholine Cytidylyltransferase Gene (Pcyt1a).
1111   Mol Cell Biol. 2005;25: 3357–3363. doi:10.1128/mcb.25.8.3357-3363.2005

1112   72.   Wang Y, Zeng C, Li J, Zhou Z, Ju X, Xia S, et al. PAK2 Haploinsufficiency Results in
1113   Synaptic Cytoskeleton Impairment and Autism-Related Behavior. Cell Rep. 2018;24:
1114   2029–2041. doi:10.1016/j.celrep.2018.07.061

1115   73.   Levy JE, Jin O, Fujiwara Y, Kuo F, Andrews NC. Transferrin receptor is necessary for
1116   development of erythrocytes and the nervous system. Nat Genet. 1999;21: 396–399.
1117   doi:10.1038/7727

1118   74.   Eicher JD, Landowski C, Stackhouse B, Sloan A, Chen W, Jensen N, et al. GRASP
1119   v2.0: An update on the Genome-Wide Repository of Associations between SNPs and
1120   Phenotypes. Nucleic Acids Res. 2015;43: D799–D804. doi:10.1093/nar/gku1202

1121   75.   Turner TN, Yi Q, Krumm N, Huddleston J, Hoekzema K, Stessman HAF, et al. NAR
1122   Breakthrough Article denovo-db: A compendium of human de novo variants. Nucleic
1123   Acids Res. 2017;45: D804–D811. doi:10.1093/nar/gkw865

1124   76.   Purcell SM, Moran JL, Fromer M, Ruderfer D, Solovieff N, Roussos P, et al. A
1125   polygenic burden of rare disruptive mutations in schizophrenia. Nature. 2014;506:
1126   185–190. doi:10.1038/nature12975

1127   77.   Abrahams BS, Arking DE, Campbell DB, Mefford HC, Morrow EM, Weiss LA, et al.
1128   SFARI Gene 2.0: A community-driven knowledgebase for the autism spectrum
1129   disorders (ASDs). Mol Autism. 2013;4: 36. doi:10.1186/2040-2392-4-36

1130   78.   Pabis M, Neufeld N, Shav-Tal Y, Neugebauer KM. Binding properties and dynamic
1131   localization of an alternative isoform of the cap-binding complex subunit CBP20.
1132   Nucleus. 2010;1: 412–21. doi:10.4161/nucl.1.5.12839

1133   79.   Maquat LE. Nonsense-mediated mRNA decay: Splicing, translation and mRNP
1134   dynamics. Nat Rev Mol Cell Biol. 2004;5: 89–99. doi:10.1038/nrm1310

1135   80.   Gonatopoulos-Pournatzis T, Cowling VH. Cap-binding complex (CBC). Biochem J.
1136   2014;458: 185–185. doi:10.1042/bj4580185

1137   81.   Xu D, Woodfield SE, Lee T V, Fan Y, Antonio C, Bergmann A. Genetic control of
1138   programmed cell death (apoptosis) in Drosophila. Fly (Austin). 2009;3: 78–90.
1139   doi:10.4161/fly.3.1.7800

1140 82. Kornbluth S, White K. Apoptosis in Drosophila: Neither fish nor fowl (nor man, nor
1141   worm). J Cell Sci. 2005;118: 1779–1787. doi:10.1242/jcs.02377

1142 83. Tittel JN, Steller H. A comparison of programmed cell death between species. Genome
1143   Biol. 2000;1: REVIEWS0003. doi:10.1186/gb-2000-1-3-reviews0003

1144 84. Bilder D, Li M, Perrimon N. Cooperative regulation of cell polarity and growth by
1145   Drosophila tumor suppressors. Science. 2000;289: 113–116.
1146   doi:10.1126/science.289.5476.113

1147 85. Humbert P, Russell S, Richardson H. Dlg, scribble and Lgl in cell polarity, cell
1148   proliferation and cancer. BioEssays. 2003;25: 542–553. doi:10.1002/bies.10286

1149 86. Shin EY, Shin KS, Lee CS, Woo KN, Quan SH, Soung NK, et al. Phosphorylation of
1150   p85 βPIX, a Rac/Cdc42-specific guanine nucleotide exchange factor, via the
1151   Ras/ERK/PAK2 pathway is required for basic fibroblast growth factor-induced neurite
1152   outgrowth. J Biol Chem. 2002;277: 44417–44430. doi:10.1074/jbc.M203754200

1153 87. Luo S, Rubinsztein DC. Huntingtin promotes cell survival by preventing Pak2
1154   cleavage. J Cell Sci. 2009;122: 875–885. doi:10.1242/jcs.050013

1155 88. Courchesne E, Mouton PR, Calhoun ME, Semendeferi K, Ahrens-Barbeau C, Hallet
1156   MJ, et al. Neuron number and size in prefrontal cortex of children with autism. JAMA
1157   - J Am Med Assoc. 2011;306: 2001–2010. doi:10.1001/jama.2011.1638

1158 89. Kreczmanski P, Heinsen H, Mantua V, Woltersdorf F, Masson T, Ulfig N, et al.
1159   Volume, neuron density and total neuron number in five subcortical regions in
1160   schizophrenia. Brain. 2007;130: 678–692. doi:10.1093/brain/awl386

1161 90. Dong D, Zielke HR, Yeh D, Yang P. Cellular stress and apoptosis contribute to the
1162   pathogenesis of autism spectrum disorder. Autism Res. 2018;11: 1076–1090.
1163   doi:10.1002/aur.1966

1164 91. Batalla A, Bargalló N, Gassó P, Molina O, Pareto D, Mas S, et al. Apoptotic markers
1165   in cultured fibroblasts correlate with brain metabolites and regional brain volume in
1166   antipsychotic-naive first-episode schizophrenia and healthy controls. Transl
1167   Psychiatry. 2015;5: e626. doi:10.1038/tp.2015.122

1168 92. Gassó P, Mas S, Molina O, Lafuente A, Bernardo M, Parellada E. Increased
1169   susceptibility to apoptosis in cultured fibroblasts from antipsychotic-naïve first-episode
1170   schizophrenia patients. J Psychiatr Res. 2014;48: 94–101.
1171   doi:10.1016/j.jpsychires.2013.09.017

1172 93. Thormann A, Halachev M, McLaren W, Moore DJ, Svinti V, Campbell A, et al.
1173   Flexible and scalable diagnostic filtering of genomic variants using G2P with Ensembl
1174   VEP. Nat Commun. 2019;10: 2373. doi:10.1038/s41467-019-10016-3

1175 94. Girirajan S, Rosenfeld JA, Coe BP, Parikh S, Friedman N, Goldstein A, et al.
1176   Phenotypic Heterogeneity of Genomic Disorders and Rare Copy-Number Variants. N
1177   Engl J Med. 2012;367: 1321–1331. doi:10.1056/NEJMoa1200395

1178 95. Lindsay EA, Vitelli F, Su H, Morishima M, Huynh T, Pramparo T, et al. Tbx1
1179   haploinsufficiency in the DiGeorge syndrome region causes aortic arch defects in
1180   mice. Nature. 2001;410: 97–101. doi:10.1038/35065105

96. Poulton CJ, Schot R, Kia SK, Jones M, Verheijen FW, Venselaar H, et al. Microcephaly with simplified gyration, epilepsy, and infantile diabetes linked to inappropriate apoptosis of neural progenitors. Am J Hum Genet. 2011;89: 265–276. doi:10.1016/j.ajhg.2011.07.006

97. Silver DL, Watkins-Chow DE, Schreck KC, Pierfelice TJ, Larson DM, Burnetti AJ, et al. The exon junction complex component Magoh controls brain size by regulating neural stem cell division. Nat Neurosci. 2010;13: 551–558. doi:10.1038/nn.2527

98. Faheem M, Naseer MI, Rasool M, Chaudhary AG, Kumosani TA, Ilyas AM, et al. Molecular genetics of human primary microcephaly: an overview. BMC Med Genomics. 2015;8: S4. doi:10.1186/1755-8794-8-S1-S4

99. Frappart P-O, Tong W-M, Demuth I, Radovanovic I, Herceg Z, Aguzzi A, et al. An essential function for NBS1 in the prevention of ataxia and cerebellar defects. Nat Med. 2005;11: 538–544. doi:10.1038/nm1228

100. Hu Y, Flockhart I, Vinayagam A, Bergwitz C, Berger B, Perrimon N, et al. An integrative approach to ortholog prediction for disease-focused and other functional studies. BMC Bioinformatics. 2011;12: 357. doi:10.1186/1471-2105-12-357

101. Mi H, Huang X, Muruganujan A, Tang H, Mills C, Kang D, et al. PANTHER version 11: expanded annotation data from Gene Ontology and Reactome pathways, and data analysis tool enhancements. Nucleic Acids Res. 2017;45: D183–D189. doi:10.1093/nar/gkw1138

102. Dietzl G, Chen D, Schnorrer F, Su K-C, Barinova Y, Fellner M, et al. A genome-wide transgenic RNAi library for conditional gene inactivation in Drosophila. Nature. 2007;448: 151–6. doi:10.1038/nature05954

103. Green EW, Fedele G, Giorgini F, Kyriacou CP. A Drosophila RNAi collection is subject to dominant phenotypic effects. Nat Methods. 2014;11: 222–223. doi:10.1038/nmeth.2856

104. Chintapalli VR, Wang J, Dow JAT. Using FlyAtlas to identify better Drosophila melanogaster models of human disease. Nat Genet. 2007;39: 715–720. doi:10.1038/ng2049

105. Graveley BR, Brooks AN, Carlson JW, Duff MO, Landolin JM, Yang L, et al. The developmental transcriptome of Drosophila melanogaster. Nature. 2011;471: 473–479. doi:10.1038/nature09715

106. Ye J, Coulouris G, Zaretskaya I, Cutcutache I, Rozen S, Madden TL. Primer-BLAST: A tool to design target-specific primers for polymerase chain reaction. BMC Bioinformatics. 2012;13: 134. doi:10.1186/1471-2105-13-134

107. Livak KJ, Schmittgen TD. Analysis of Relative Gene Expression Data Using Real-Time Quantitative PCR and the $2-\Delta\Delta CT$ Method. Methods. 2001;25: 402–408. doi:10.1006/meth.2001.1262

108. Schneider CA, Rasband WS, Eliceiri KW. NIH Image to ImageJ: 25 years of image analysis. Nat Methods. 2012;9: 671–675. doi:10.1038/nmeth.2089

109. Bolger AM, Lohse M, Usadel B. Trimmomatic: A flexible trimmer for Illumina

1222   sequence data. Bioinformatics. 2014;30: 2114–2120.
1223   doi:10.1093/bioinformatics/btu170

1224   110.   Kim D, Pertea G, Trapnell C, Pimentel H, Kelley R, Salzberg SL. TopHat2: accurate
1225   alignment of transcriptomes in the presence of insertions, deletions and gene fusions.
1226   Genome Biol. 2013;14: R36. doi:10.1186/gb-2013-14-4-r36

1227   111.   Anders S, Pyl PT, Huber W. HTSeq-A Python framework to work with high-
1228   throughput sequencing data. Bioinformatics. 2015;31: 166–169.
1229   doi:10.1093/bioinformatics/btu638

1230   112.   Robinson MD, McCarthy DJ, Smyth GK. edgeR: A Bioconductor package for
1231   differential expression analysis of digital gene expression data. Bioinformatics.
1232   2009;26: 139–140. doi:10.1093/bioinformatics/btp616

1233   113.   Dougherty JD, Schmidt EF, Nakajima M, Heintz N. Analytical approaches to RNA
1234   profiling data for the identification of genes enriched in specific cells. Nucleic Acids
1235   Res. 2010;38: 4218–4230. doi:10.1093/nar/gkq130

1236   114.   Miller JA, Ding S-L, Sunkin SM, Smith KA, Ng L, Szafer A, et al. Transcriptional
1237   landscape of the prenatal human brain. Nature. 2014;508: 199–206.
1238   doi:10.1038/nature13185

1239   115.   Sive HL, Grainger RM, Harland RM. Microinjection of Xenopus Oocytes. Cold
1240   Spring Harb Protoc. 2010;2010: pdb.prot5536. doi:10.1101/pdb.prot5536

1241   116.   Lowery LA, Faris AER, Stout A, Van Vactor D. Neural Explant Cultures from
1242   Xenopus laevis. J Vis Exp. 2012; e4232. doi:10.3791/4232

1243   117.   Nieuwkoop PD, Faber J. Normal table of Xenopus laevis (Daudin) : a systematical and
1244   chronological survey of the development from the fertilized egg till the end of
1245   metamorphosis. New York : Garland Pub; 1994.

1246   118.   Hagberg AA, Schult DA, Swart PJ. Exploring network structure, dynamics, and
1247   function using NetworkX. 7th Python in Science Conference (SciPy 2008). 2008. pp.
1248   11–15.

1249   119.   Carbon S, Ireland A, Mungall CJ, Shu S, Marshall B, Lewis S, et al. AmiGO: Online
1250   access to ontology and annotation data. Bioinformatics. 2009;25: 288–289.
1251   doi:10.1093/bioinformatics/btn615

1252   120.   Karimi K, Fortriede JD, Lotay VS, Burns KA, Wang DZ, Fisher ME, et al. Xenbase: A
1253   genomic, epigenomic and transcriptomic model organism database. Nucleic Acids Res.
1254   2018;46: D861–D868. doi:10.1093/nar/gkx936

1255   121.   Greenwood S, Struhl G. Progression of the morphogenetic furrow in the Drosophila
1256   eye: The roles of Hedgehog, Decapentaplegic and the Raf pathway. Development.
1257   1999;126: 5795–5808.

1258   122.   Thurmond J, Goodman JL, Strelets VB, Attrill H, Gramates LS, Marygold SJ, et al.
1259   FlyBase 2.0: The next generation. Nucleic Acids Res. 2019;47: D759–D765.
1260   doi:10.1093/nar/gky1003

1261   123.   Bult CJ, Blake JA, Smith CL, Kadin JA, Richardson JE, Anagnostopoulos A, et al.

Mouse Genome Database (MGD) 2019. Nucleic Acids Res. 2019;47: D801–D806. doi:10.1093/nar/gky1056

124. Petrovski S, Wang Q, Heinzen EL, Allen AS, Goldstein DB. Genic Intolerance to Functional Variation and the Interpretation of Personal Genomes. PLoS Genet. 2013;9: e1003709. doi:10.1371/journal.pgen.1003709

125. Lek M, Karczewski KJ, Minikel E V., Samocha KE, Banks E, Fennell T, et al. Analysis of protein-coding genetic variation in 60,706 humans. Nature. 2016;536: 285–291. doi:10.1038/nature19057

126. O'Leary NA, Wright MW, Brister JR, Ciufo S, Haddad D, McVeigh R, et al. Reference sequence (RefSeq) database at NCBI: Current status, taxonomic expansion, and functional annotation. Nucleic Acids Res. 2016;44: D733–D745. doi:10.1093/nar/gkv1189

127. UniProt Consortium. UniProt: the universal protein knowledgebase. Nucleic Acids Res. 2018;46: 2699–2699. doi:10.1093/nar/gky092

128. The Gene Ontology Consortium. The Gene Ontology Resource: 20 years and still GOing strong. Nucleic Acids Res. 2019;47: D330–D338. doi:10.1093/nar/gky1055

1279 **FIGURE LEGENDS**

1280 **Fig. 1. Strategy for identifying cellular phenotypes and genetic interactions of homologs**

1281 **of 3q29 genes.**

1282 We first knocked down individual or pairs of 14 *Drosophila* homologs of human genes in the

1283 3q29 region using tissue-specific RNAi. After screening for global phenotypes of RNAi lines

1284 for individual homologs of 3q29 genes, we tested 314 pairwise gene interactions using the fly

1285 eye, and found that *Cbp20* (*NCBP2*) enhanced the phenotypes of other homologs of 3q29

1286 genes and also interacted with homologs of known neurodevelopmental genes outside of the

1287 3q29 region. Next, we assayed for deeper cellular and neuronal phenotypes of flies with

1288 individual and pairwise knockdown of homologs of 3q29 genes, and observed cellular defects

1289 due to disrupted apoptosis and cell cycle mechanisms. We confirmed our results by rescuing

1290 cellular phenotypes with overexpression of the apoptosis inhibitor *Diap1* and by analyzing

1291 genes differentially expressed with knockdown of homologs of 3q29 genes. Finally, we tested

1292 a subset of three homologs of 3q29 genes in the *X. laevis* vertebrate model system by

1293 injecting two- or four-cell stage embryos with GFP and morpholinos (MOs) for *X. laevis*

1294 homologs of 3q29 genes to observe abnormal eye morphology, as well as injecting one cell

1295 with GFP and MOs at the two-cell stage to observe abnormal brain morphology. We found

1296 similar developmental defects in *X. laevis* to those observed in *Drosophila*, including

1297 increased apoptosis that was enhanced with pairwise knockdown of homologs of 3q29 genes

1298 and rescued with overexpression of the apoptosis inhibitor *xiap*. *X. laevis* embryo diagrams

1299 were produced by Nieuwkoop and Faber [117] and provided by Xenbase [120].

1300

1301 **Fig. 2**. **Neurodevelopmental defects in flies with knockdown of individual homologs of**

1302 **3q29 genes.**

1303 (**A**) Percentage of flies with tissue-specific RNAi knockdown of homologs of 3q29 genes

1304 (listed with their human counterparts) that manifest lethality or developmental phenotypes.

1305 (**B**) Eight homologs of 3q29 genes with pan-neuronal RNAi knockdown showed defects in

1306 climbing ability over ten days (two-way repeated measures ANOVA, $p < 1 \times 10^{-4}$, df $= 8$,

1307 F $= 21.097$). Data represented show mean $\pm$ standard deviation of 10 independent groups of

1308 10 flies for each homolog. (**C**) Representative brightfield adult eye images of flies with eye-

1309 specific *GMR-GAL4;UAS-Dicer2* (scale bar $= 100\ \mu m$) RNAi knockdown of individual

1310 homologs of 3q29 genes show rough eye phenotypes. The boxplot shows *Flynotyper*-derived

1311 phenotypic scores for eyes with knockdown of homologs of 3q29 genes (n $= 10$–14,

1312 *p < 0.05, one-tailed Mann–Whitney test with Benjamini-Hochberg correction). (**D**) Boxplot

40

1313   of adult eye area in flies with *GMR-GAL4* RNAi knockdown of fly homologs of 3q29 genes

1314   (n = 13–16, *p < 0.05, two-tailed Mann–Whitney test with Benjamini-Hochberg correction).

1315   (**E**) Confocal images of pupal eyes (scale bar = 5 µm) stained with anti-DLG (top) and larval

1316   eye discs (scale bar = 30 µm) stained with anti-pH3 (middle) and anti-dcp1 (bottom) illustrate

1317   cellular defects posterior to the morphogenetic furrow (white box) upon knockdown of select

1318   fly homologs of 3q29 genes. Yellow circles in DLG images indicate cone cell defects, white

1319   circles indicate bristle cell defects, yellow arrows indicate rotation defects, and yellow

1320   arrowheads indicate secondary cell defects. We note that pupal eye images were taken at a

1321   higher intensity for lines with knockdown of *dlg1* to account for reduced expression of DLG

1322   (see Methods), as these images were only for visualization of cell boundaries in the pupal eye

1323   and not for any quantitative analysis. (**F**) Boxplot of pH3-positive cells in larval eye discs of

1324   flies with knockdown of homologs of 3q29 genes (n = 9–12, *p < 0.05, two-tailed Mann–

1325   Whitney test with Benjamini-Hochberg correction). (**G**) Boxplot of dcp1-positive cells in

1326   larval eye discs of flies with knockdown of homologs of 3q29 genes (n = 11–12, *p < 0.05,

1327   two-tailed Mann–Whitney test with Benjamini-Hochberg correction). All boxplots indicate

1328   median (center line), 25th and 75th percentiles (bounds of box), and minimum and maximum

1329   (whiskers), with red dotted lines representing the control median. Results for a subset of

1330   climbing ability, adult eye area, and pH3 staining experiments were replicated in independent

1331   experimental batches (**S14 Fig.**). A list of full genotypes for fly crosses used in these

1332   experiments is provided in **S2 File**.

1333

1334   **Fig. 3**. **Screening for pairwise interactions of fly homologs of 3q29 genes in the**

1335   ***Drosophila* eye and nervous system.**

1336   (**A**) Heatmap showing average changes in phenotypic scores for pairwise *GMR-GAL4* RNAi

1337   knockdown of fly homologs of 3q29 genes in the adult eye, compared with recombined lines

1338   for individual homologs of 3q29 genes crossed with controls. Gray boxes indicate crosses

1339   without available data. Boxplots of phenotypic scores for pairwise knockdown of (**B**) *Cbp20*

1340   and (**C**) *dlg1* with other fly homologs of 3q29 genes are shown (n = 5–14, *p < 0.05, two-

1341   tailed Mann–Whitney test with Benjamini-Hochberg correction). Green arrows indicate an

1342   example pair of reciprocal lines showing enhanced phenotypes compared with their

1343   respective single-hit recombined controls. Crosses with the mutant line *Tsf2*^{KG01571} are

1344   included along with RNAi lines for other homologs of 3q29 genes, as eye-specific RNAi

1345   knockdown of *Tsf2* was lethal. (**D**) Representative brightfield adult eye images of flies with

1346   pairwise knockdown of fly homologs of 3q29 genes (scale bar = 100 µm) show enhancement

41

1347 (Enh.) of rough eye phenotypes compared with recombined lines for individual homologs of

1348 3q29 genes crossed with controls. (**E**) Representative confocal images of larval eye discs

1349 stained with anti-chaoptin (scale bar = 30 μm) illustrate enhanced defects (Enh.) in axon

1350 targeting (white arrows) from the retina to the optic lobes of the brain with eye-specific

1351 knockdown of *Cbp20/dlg1* and *Cbp20/Fsn* compared with *Cbp20* knockdown. Note that n=9-

1352 17 larval eye disc preparations were assessed for each tested interaction. (**F**) Flies with pan-

1353 neuronal *Elav-GAL4* pairwise knockdown of homologs of 3q29 genes showed enhanced

1354 defects in climbing ability over ten days (two-way repeated measures ANOVA, $p < 4.00 \times 10^{-4}$,

1355 df = 2, F = 7.966) compared with recombined *Cbp20* knockdown crossed with control. Data

1356 represented show mean ± standard deviation of 10 independent groups of 10 flies for each

1357 line tested. Results for the climbing assays were replicated in an independent experimental

1358 batch (**S14 Fig.**). All boxplots indicate median (center line), 25th and 75th percentiles

1359 (bounds of box), and minimum and maximum (whiskers), with red dotted lines representing

1360 the control median. A list of full genotypes for fly crosses used in these experiments is

1361 provided in **S2 File**.

1362

1363 **Fig. 4. Connectivity of 3q29 genes in human gene interaction databases.**

1364 (**A**) Genetic interactions of 3q29 genes in the context of a general human gene interaction

1365 network (GeneMania). The strongly connected component includes 11/21 total 3q29 genes.

1366 Black-shaded nodes represent the input 3q29 genes, while grey nodes represent connector

1367 genes in the network. Edge color represents the interaction data source (purple: co-

1368 expression, orange: predicted interaction), while edge thickness represents weighted scores

1369 for each interaction. (**B**) Genetic interactions of 19 genes in the 3q29 region in the context of

1370 a brain-specific human gene interaction network (GIANT). Large nodes represent the input

1371 3q29 genes, while small nodes represent connector genes in the network. Edge color

1372 represents the weighted score for each interaction, from low connectivity (green) to high

1373 connectivity (red). (**C**) Histograms and smoothed normal distributions showing the average

1374 connectivity among genes in the 3q29 region (blue) along with two other large CNVs,

1375 16p11.2 (red) and 22q11.2 deletion (green), within a brain-specific gene interaction network.

1376 Average connectivity is measured as the shortest weighted distance between two genes, with

1377 lower distances representing higher connectivity. Genes within the 3q29 and 22q11.2

1378 deletions were not significantly more connected to each other (p>0.05, one-tailed Mann-

1379 Whitney test with Benjamini-Hochberg correction) than random sets of 21 genes throughout

1380 the genome (grey). However, genes within the 16p11.2 region were significantly more

1381   connected to each other than the random gene sets (p=0.003, one-tailed Mann-Whitney test

1382   with Benjamini-Hochberg correction). (**D**) Pairwise connectivity of individual 3q29 genes

1383   within a brain-specific gene interaction network, excluding six genes not present in the

1384   network (*RNF168*, *ZDHHC19*, *LRRC33*, *OSTalpha*, *SMCO1*, and *TCTEX1D2*). Average

1385   connectivity is measured as the shortest weighted distance between two genes, with lower

1386   values representing higher connectivity. Underlined genes have a higher average connectivity

1387   (p<0.05, one-tailed Mann-Whitney test with Benjamini-Hochberg correction) to other genes

1388   in the region compared with random sets of 21 genes throughout the genome.

1389

1390   **Fig. 5**. **Cellular phenotypes with pairwise knockdown of fly homologs of 3q29 genes.**

1391   (**A**) Representative brightfield adult eye images (scale bar = 100 µm) show that heterozygous

1392   *GMR-GAL4* RNAi knockdown of *dlg1* enhanced the rough eye phenotype and necrotic

1393   patches (yellow circles) of flies heterozygous or homozygous for *Cbp20* RNAi. (**B**)

1394   Representative confocal images of pupal eyes (scale bar = 5 µm) stained with anti-DLG

1395   illustrate enhanced defects in ommatidial organization upon concomitant knockdown of

1396   *Cbp20* with other fly homologs of 3q29 genes compared with *Cbp20* knockdown. Yellow

1397   circles in DLG images indicate cone cell defects, white circles indicate bristle cell defects,

1398   yellow arrows indicate rotation defects, and yellow arrowheads indicate secondary cell

1399   defects. We note that pupal eye images were taken at a higher intensity for lines with

1400   knockdown of *Cbp20*/*dlg1* to account for reduced expression of DLG (see Methods), as these

1401   images were only for visualization of cell boundaries in the pupal eye and not for any

1402   quantitative analysis. (**C**) Representative confocal images of pupal eyes (scale bar = 5 µm)

1403   stained with Phalloidin illustrate enhanced defects in photoreceptor cell count and

1404   organization upon concomitant knockdown of *Cbp20* and other fly homologs of 3q29 genes

1405   compared with *Cbp20* knockdown. (**D**) Representative confocal images of larval eye discs

1406   (scale bar = 30 µm) stained with anti-dcp1 (top) and anti-pH3 (bottom) show enhanced

1407   defects in apoptosis and cell proliferation with pairwise knockdown of *Cbp20* and other fly

1408   homologs of 3q29 genes compared with recombined *Cbp20* knockdown crossed with

1409   controls. (**E**) Boxplot of dcp1-positive cells in the larval eye discs of flies with pairwise

1410   knockdown of homologs of 3q29 genes (n = 10–11, *p < 0.05, two-tailed Mann–Whitney test

1411   with Benjamini-Hochberg correction). (**F**) Boxplot of pH3-positive cells in the larval eye

1412   discs of flies with pairwise knockdown of homologs of 3q29 genes (n = 10–12, *p < 0.05,

1413   two-tailed Mann–Whitney test with Benjamini-Hochberg correction). All boxplots indicate

1414   median (center line), 25th and 75th percentiles (bounds of box), and minimum and maximum

1415   (whiskers), with red dotted lines representing the control median. A list of full genotypes for

1416   fly crosses used in these experiments is provided in **S2 File**.

1417

1418   **Fig. 6**. **Rescue of cellular phenotypes due to knockdown of fly homologs of 3q29 genes**

1419   **with overexpression of the apoptosis inhibitor *Diap1*.**

1420   (**A**) Representative brightfield adult eye images (scale bar = 100 μm) show rescue of rough

1421   eye phenotypes for flies with concomitant *GMR-GAL4* RNAi knockdown of *Cbp20* or *dlg1*

1422   and overexpression of *Diap1*, as well as enhanced (Enh.) phenotypes with overexpression of

1423   caspase-9 homolog *Dronc*. (**B**) Boxplot of phenotypic scores for flies with knockdown of

1424   *Cbp20* or *dlg1* and overexpression of *Diap1* or *Dronc* (n = 8–9, *p < 0.05, two-tailed Mann–

1425   Whitney test with Benjamini-Hochberg correction) is shown. (**C**) Box plot showing area of

1426   necrotic patches in adult fly eyes with knockdown of *Cbp20* and overexpression of *Dronc*

1427   (n=9, *p=1.14×10^{-4}, one-tailed Mann–Whitney test with Benjamini-Hochberg correction) is

1428   shown. (**D**) Confocal images of pupal eyes (scale bar = 5 μm) stained with anti-DLG illustrate

1429   the rescue of ommatidial organization defects due to knockdown of *Cbp20* or *dlg1* upon

1430   overexpression of *Diap1*. Yellow circles in DLG images indicate cone cell defects, white

1431   circles indicate bristle cell defects, yellow arrows indicate rotation defects, and yellow

1432   arrowheads indicate secondary cell defects. We note that pupal eye images were taken at a

1433   higher intensity for lines with knockdown of *dlg1* to account for reduced expression of DLG

1434   (see Methods), as these images were only for visualization of cell boundaries in the pupal eye

1435   and not for any quantitative analysis. (**E**) Larval eye discs (scale bar = 30 μm) stained with

1436   anti-dcp1 show rescue of apoptosis phenotypes observed in flies with *Cbp20* and *dlg1*

1437   knockdown upon *Diap1* overexpression as well as enhanced (Enh.) phenotypes upon *Dronc*

1438   overexpression. (**F**) Boxplot of dcp1-positive cells in the larval eye discs of flies with

1439   knockdown of *Cbp20* or *dlg1* and *Diap1* or *Dronc* overexpression (n = 9–18, *p < 0.05, two-

1440   tailed Mann–Whitney test with Benjamini-Hochberg correction). (**G**) Representative confocal

1441   images of larval eye discs stained with anti-chaoptin (scale bar = 30 μm) illustrate the

1442   suppression (Supp.) of axon targeting defects (white arrows) observed in flies due to

1443   knockdown of *Cbp20* or *dlg1* with overexpression of *Diap1*. Note that n=8-18 larval eye disc

1444   preparations were assessed for each interaction cross tested. All boxplots indicate median

1445   (center line), 25th and 75th percentiles (bounds of box), and minimum and maximum

1446   (whiskers), with red dotted lines representing the control median. A list of full genotypes for

1447   fly crosses used in these experiments is provided in **S2 File**.

1448

1449 **Fig. 7. Pairwise interactions between fly homologs of 3q29 genes and other**

1450 **neurodevelopmental genes.**

1451 (**A**) Heatmap showing the average changes in phenotypic scores for the *GMR-GAL4* pairwise

1452 RNAi knockdown of fly homologs for 3q29 genes and other neurodevelopmental genes

1453 (along with their human counterparts) in the adult eye, compared with recombined lines for

1454 individual homologs of 3q29 genes crossed with controls. (**B**) Representative brightfield adult

1455 eye images of flies with pairwise knockdown of fly homologs for 3q29 genes and known

1456 neurodevelopmental genes (scale bar = 100 µm) show enhancement (Enh.) or suppression

1457 (Supp.) of rough eye phenotypes and necrotic patches compared with flies with knockdown

1458 of individual homologs of neurodevelopmental genes. A list of full genotypes for fly crosses

1459 used in these experiments is provided in **S2 File**.

1460

1461 **Fig. 8. Developmental phenotypes observed with knockdown of homologs of 3q29 genes**

1462 **in *X. laevis* models.**

1463 (**A**) To study brain morphology upon knockdown of *X. laevis* homologs of genes in the 3q29

1464 region, one cell in a two-cell embryo was injected with single or multiple MOs for homologs

1465 of 3q29 genes while the other cell remained uninjected. Representative images of stage 47 *X.*

1466 *laevis* tadpoles (scale bar = 500 µm) with MO knockdown of *ncbp2, fxbo45* and *pak2* show

1467 morphological defects and decreased size, including decreased forebrain (highlighted in red

1468 on the control image) and midbrain (highlighted in yellow) area, compared with control

1469 tadpoles. Pairwise knockdown of *fbxo45* and *ncbp2* enhanced these phenotypes, which were

1470 also rescued with overexpression of *xiap*. (**B**) Box plot of forebrain area in *X. laevis* models

1471 with knockdown of homologs of 3q29 genes, normalized to controls (n = 30–63, *p < 0.05,

1472 two-tailed Welch's T-test with Benjamini-Hochberg correction). Red box indicates rescue of

1473 decreased *ncbp2* forebrain area with overexpression of the apoptosis inhibitor *xiap*. (**C**) Box

1474 plot of midbrain area in *X. laevis* models with knockdown of homologs of 3q29 genes,

1475 normalized to controls (n = 30–63, *p < 0.05, two-tailed Welch's T-test with Benjamini-

1476 Hochberg correction). Red box indicates rescue of decreased *ncbp2* midbrain area with

1477 overexpression of the apoptosis inhibitor *xiap*. (**D**) Western blot analysis of *X. laevis* whole

1478 embryos show increased intensity of cleaved caspase-3 bands at 19kD and 17kD with

1479 knockdown of homologs of 3q29 genes, including enhanced caspase-3 levels with

1480 knockdown of multiple homologs of 3q29 genes and rescued levels with *xiap* overexpression.

1481 β-actin was used as a loading control on the same blot. Representative western blot images

1482 shown are cropped; the full blots for both replicates are provided in **S12 Fig**. (**E**)

45

1483 Quantification of western blot band intensity for caspase-3 levels, normalized to the loading

1484 control. Red box indicates rescue of increased caspase-3 levels with overexpression of the

1485 apoptosis inhibitor *xiap*. All boxplots indicate median (center line), 25th and 75th percentiles

1486 (bounds of box), and minimum and maximum (whiskers), with red dotted lines representing

1487 the control median. The data shown for the brain area experiments represent pooled results of

1488 three experimental batches, and were normalized to the respective controls from each batch.

1489 *X. laevis* embryo diagrams were produced by Nieuwkoop and Farber [117] and provided by

1490 Xenbase [120].

1491

1492 **Fig. 9. Interactions between *NCBP2* and other homologs of 3q29 genes contribute to**

1493 **neurodevelopmental defects through conserved cellular pathways.**

1494 **(A)** We identified 44 interactions between pairs of *Drosophila* homologs of 3q29 genes. With

1495 the exception of *Ulp1* (*SENP5*)*,* the cellular phenotypes of each homolog were significantly

1496 enhanced with simultaneous knockdown of *Cbp20*. While other homologs of 3q29 genes also

1497 interact with each other, our data suggest that *Cbp20* is a key modulator of cellular

1498 phenotypes within the deletion region. **(B)** Schematic representing the network context of

1499 *NCBP2* and other genes in the 3q29 region towards neurodevelopmental phenotypes. We

1500 propose that the effects of *NCBP2* disruption propagate through a network of functionally-

1501 related genes, including other 3q29 genes (highlighted in blue), leading to a cascade of

1502 disruptions in key biological mechanisms, including apoptosis and cell cycle pathways. These

1503 pathways jointly contribute towards the observed neurodevelopmental phenotypes.

1504

46

1505 **SUPPORTING INFORMATION LEGENDS**

1506 **S1 Fig. Developmental defects in flies with tissue-specific knockdown of individual**

1507 **homologs of 3q29 genes.**

1508 (**A**) Images of adult fly wings (scale bar = 500um) show a range of phenotypic defects due to

1509 wing-specific bx^{MS1096}-GAL4 RNAi knockdown of fly homologs of 3q29 genes. (**B**) Adult

1510 flies with pan-neuronal RNAi knockdown of *dlg1* showed approximately 30% lethality

1511 between days 1-4 (one-way repeated measures ANOVA, $p<1\times10^{-4}$, df = 1, F = 54.230), which

1512 was not observed in control *Elav-GAL4* or *Cbp20* knockdown flies. Data represented shows

1513 mean ± standard deviation of 10 independent groups of 10 flies for each homolog. (**C**)

1514 Representative confocal images of larval eye discs stained with anti-chaoptin (scale

1515 bar = 30 μm) illustrate defects in axon targeting (highlighted by white arrows) from the retina

1516 to the optic lobes of the brain upon eye-specific knockdown of fly homologs of 3q29 genes.

1517 Note that n=8-20 larval eye disc preparations were assessed for each RNAi line tested. A list

1518 of full genotypes for fly crosses used in these experiments is provided in **S2 File**.

1519

1520 **S2 Fig. Examination of cellular phenotypes in the *Drosophila* eye.**

1521 We tested individual and pairwise knockdown of fly homologs of 3q29 genes for cellular

1522 phenotypes in the adult, pupal and larval eyes. (**A**) We first used the *Flynotyper* software [53]

1523 to quantify the degree of ommatidial disorganization leading to rough eye phenotypes in adult

1524 flies, as represented by the distance and angles between adjacent ommatidia (yellow arrows).

1525 (**B**) We next stained pupal eyes with anti-DLG to observe changes in the number and

1526 arrangement of ommatidial cells, including cone cells (c), bristle cells (b), and primary,

1527 secondary and tertiary cells (1,2,3). We also examined the organization of the photoreceptor

1528 cells (R1-R7, with R8 not visible) in each ommatidium by staining the pupal eyes with

1529 Phalloidin. (**C**) We finally stained larval eye discs with markers for cellular processes, such

1530 as pH3 for proliferating cells and dcp1 for apoptosis. As the progression of the

1531 morphogenetic furrow (MF) across the larval eye discs leads to proliferation and

1532 differentiation of photoreceptor neurons [121], we examined changes in the number of

1533 stained cells posterior to the MF. (**D**) Scatter plot of dcp1, pH3, TUNEL, and BrdU-positive

1534 cell counts in larval eye discs with knockdown of homologs of 3q29 genes quantified using

1535 two ImageJ plugins, AnalyzeParticles and Image-based Tool for Counting Nuclei (ITCN). As

1536 the two methods showed a strong correlation with each other (Pearson correlation, n=285,

1537 r=0.736, $p<2.2\times10^{-16}$), we used ITCN counts to display cell count data in the manuscript.

1538

47

S3 Fig. Phenotypic screening for flies with eye-specific knockdown of individual fly homologs of 3q29 genes.

(**A**) Representative brightfield adult eye images of flies with *GMR-GAL4;UAS-Dicer2* RNAi knockdown of fly homologs of 3q29 genes (scale bar = 100 µm) show a wide range of phenotypic severity. (**B**) Box plot of average ommatidial diameter in flies with *GMR-GAL4* knockdown of select fly homologs of 3q29 genes is shown (n = 15, *p < 0.05, two-tailed Mann–Whitney test with Benjamini-Hochberg correction). (**C**) Box plot of phenotypic scores derived from *Flynotyper* for eye-specific *dCad-GFP,GMR-GAL4* RNAi knockdown of 13 fly homologs of 3q29 genes is shown (n = 5–20, *p < 0.05, one-tailed Mann–Whitney test with Benjamini-Hochberg correction). (**D**) Box plot of phenotypic scores derived from *Flynotyper* for eye-specific *GMR-GAL4;UAS-Dicer2* (left) and *dCad-GFP,GMR-GAL4* (right) RNAi knockdown of nine validation lines for fly homologs of 3q29 genes is shown (n = 5–14, *p < 0.05, one-tailed Mann–Whitney test with Benjamini-Hochberg correction). All boxplots indicate median (center line), 25th and 75th percentiles (bounds of box), and minimum and maximum (whiskers), with red dotted lines representing the control median. A list of full genotypes for fly crosses used in these experiments is provided in **S2 File**.

S4 Fig. Cellular phenotypes of flies with eye-specific knockdown of individual fly homologs of 3q29 genes.

(**A**) Confocal images of pupal eyes (scale bar = 5 µm) stained with anti-DLG illustrate a range of defects in ommatidial organization upon *GMR-GAL4* RNAi knockdown of fly homologs of 3q29 genes. Yellow circles indicate cone cell defects, white circles indicate bristle cell defects, yellow arrows indicate rotation defects, and yellow arrowheads indicate secondary cell defects. (**B**) Confocal images of pupal eyes (scale bar = 5 µm) stained with Phalloidin illustrate defects in photoreceptor cell count and organization upon knockdown of fly homologs of 3q29 genes. (**C**) Confocal images of larval eye discs (scale bar = 30 µm) stained with anti-pH3 illustrate changes in cell proliferation upon knockdown of select fly homologs of 3q29 genes. (**D**) Larval eye discs (scale bar = 30 µm) stained with BrdU (top) and TUNEL (bottom) illustrate abnormal cell cycle and apoptosis defects, respectively, due to eye-specific knockdown of *Cbp20* and *dlg1*. (**E**) Box plot of BrdU-positive cells in the larval eye discs of flies with knockdown of *dlg1* and *Cbp20* is shown (n = 7–12, *p < 0.05, two-tailed Mann–Whitney test with Benjamini-Hochberg correction). (**F**) Box plot of TUNEL-positive cells in the larval eye discs of flies with knockdown of *dlg1* and *Cbp20* is shown (n = 8, *p < 0.05, two-tailed Mann–Whitney test with Benjamini-Hochberg correction). Results for the TUNEL

48

1573 staining experiments were replicated in an independent experimental batch (**S14 Fig.**). All

1574 boxplots indicate median (center line), 25th and 75th percentiles (bounds of box), and

1575 minimum and maximum (whiskers), with red dotted lines representing the control median. A

1576 list of full genotypes for fly crosses used in these experiments is provided in **S2 File**.

1577

1578 **S5 Fig. Cellular phenotypes of flies with wing-specific knockdown of individual fly**

1579 **homologs of 3q29 genes.**

1580 (**A**) Larval wing discs (scale bar = 50 μm) stained with pH3 illustrate abnormal cell

1581 proliferation due to RNAi knockdown of select fly homologs of 3q29 genes, compared with

1582 appropriate VDRC GD and KK *bx*^{MS1096}*-GAL4* controls. We examined changes in the number

1583 of stained cells within the wing pouch of the wing disc (white box), which becomes the adult

1584 wing. (**B**) Box plot of pH3-positive cells in the larval wing discs of flies with knockdown of

1585 select fly homologs of 3q29 genes is shown (n = 8–15, *$p < 0.05$, two-tailed Mann–Whitney

1586 test with Benjamini-Hochberg correction). (**C**) Larval wing discs (scale bar = 50 μm) stained

1587 with anti-dcp1 show abnormal apoptosis due to knockdown of select fly homologs of 3q29

1588 genes compared with appropriate VDRC GD and KK *bx*^{MS1096}*-GAL4* controls. (**D**) Box plot

1589 of dcp1-positive cells in the larval wing discs of flies with knockdown of select fly homologs

1590 of 3q29 genes is shown (n = 8–15, *$p < 0.05$, two-tailed Mann–Whitney test with Benjamini-

1591 Hochberg correction). *Cbp20* flies showed severe dcp1 staining across the entire wing pouch

1592 and could not be quantified. All boxplots indicate median (center line), 25th and 75th

1593 percentiles (bounds of box), and minimum and maximum (whiskers), with red dotted lines

1594 representing the control median. A list of full genotypes for fly crosses used in these

1595 experiments is provided in **S2 File**.

1596

1597 **S6 Fig. Phenotypic screening for pairwise interactions of homologs of 3q29 genes in the**

1598 **adult fly eye.**

1599 (**A**) Heatmap showing average changes in phenotypic scores for pairwise *GMR-GAL4* RNAi

1600 knockdown of fly homologs of 3q29 genes in the adult eye, compared with recombined lines

1601 for individual homologs of 3q29 genes crossed with controls, is shown. Gray boxes indicate

1602 crosses without available data. Crosses with the mutant line *Tsf2*^{KG01571} are also included

1603 along with RNAi lines for other homologs of 3q29 genes, as eye-specific RNAi knockdown

1604 of *Tsf2* was lethal. (**B-H**) Box plots of phenotypic scores for pairwise knockdowns of

1605 homologs of 3q29 genes compared with recombined lines for individual homologs of 3q29

1606 genes crossed with controls are shown (n = 5–12, *$p < 0.05$, two-tailed Mann–Whitney test

49

1607   with Benjamini-Hochberg correction). All boxplots indicate median (center line), 25th and

1608   75th percentiles (bounds of box), and minimum and maximum (whiskers), with red dotted

1609   lines representing the control median. A list of full genotypes for fly crosses used in these

1610   experiments is provided in **S2 File**.

1611

1612   **S7 Fig. Validation lines for pairwise interactions of homologs of 3q29 genes in the adult**

1613   **fly eye.**

1614   (**A-F**) Box plots of phenotypic scores for pairwise *GMR-GAL4* RNAi knockdown of select

1615   fly homologs of 3q29 genes (*Cbp20, CG8888, dlg1, Fsn, Pak,* and *PIG-Z*) with validation

1616   RNAi and mutant lines for other homologs of 3q29 genes, compared with recombined lines

1617   for individual homologs of 3q29 genes crossed with controls, are shown (n = 4–14, *p < 0.05,

1618   two-tailed Mann–Whitney test with Benjamini-Hochberg correction), are shown. These

1619   crosses include flies homozygous for *Cbp20* RNAi as well as flies homozygous for *Cbp20*

1620   RNAi and heterozygous for *dlg1* RNAi (green arrows). Note that the phenotypic scores

1621   derived from *Flynotyper* may not accurately capture the necrotic patches observed in these

1622   crosses. All boxplots indicate median (center line), 25th and 75th percentiles (bounds of box),

1623   and minimum and maximum (whiskers), with red dotted lines representing the control

1624   median. A list of full genotypes for fly crosses used in these experiments is provided in **S2**

1625   **File**.

1626

1627   **S8 Fig. Transcriptome analysis of flies with knockdown of select homologs of 3q29**

1628   **genes.**

1629   (**A**) Clusters of Gene Ontology terms enriched among differentially-expressed fly genes

1630   (blue) and their corresponding human homologs (red) with individual and pairwise *Elav-*

1631   *GAL4* RNAi knockdown of fly homologs of 3q29 genes (p< 0.05, Fisher's Exact test with

1632   Benjamini-Hochberg correction) are shown. Black boxes indicate enrichment of each gene

1633   set for clusters of Gene Ontology terms. Full lists of enriched GO terms are provided in **S3**

1634   **File**. (**B**) Enrichments for shared and unique differentially-expressed fly genes (blue) and

1635   their corresponding human homologs (red) with individual knockdown of *Cbp20* and *Fsn*, as

1636   well as concomitant knockdown of *Cbp20/Fsn*, are shown. We found 229 genes uniquely

1637   dysregulated in flies with pairwise knockdown of *Fsn and Cbp20*, which were enriched for

1638   cell cycle function (p=0.011 for fly gene enrichment and p=1.12×10^{-8} for human homologs,

1639   Fisher's Exact test with Benjamini-Hochberg correction). (**C**) Diagram showing human cell

1640   cycle and apoptosis genes whose fly homologs are differentially expressed with knockdown

1641   of *Cbp20* and *Fsn*, as well as concomitant knockdown of *Cbp20/Fsn*. Red boxes indicate

1642   apoptosis genes, green boxes indicate cell cycle genes, and yellow boxes indicate genes

1643   associated with both functions. (**D**) Enrichments of human homologs of genes differentially

1644   expressed in flies with knockdown of *Cbp20/Fsn* across different brain tissues and

1645   developmental timepoints are shown (Specific Expression Analysis). The size of each

1646   hexagon represents the number of genes preferentially expressed at each tissue and timepoint,

1647   with concentric hexagons representing bins of genes with stronger levels of preferential

1648   expression. The shading of each hexagon represents the enrichment of differentially-

1649   expressed genes among genes preferentially expressed at each timepoint (p<0.1, Fisher's

1650   Exact test with Benjamini-Hochberg correction). A list of full genotypes for fly crosses used

1651   in these experiments is provided in **S2 File**.

1652

1653   **S9 Fig. Cellular phenotypes for pairwise knockdowns of homologs of 3q29 genes.**

1654   (**A**) Box plot showing the area of necrotic patches in adult fly eyes with pairwise knockdown

1655   of homologs of 3q29 genes (n=5-13, *p < 0.05, one-tailed Mann–Whitney test with

1656   Benjamini-Hochberg correction). Flies with knockdown of *Cbp20* and *Fsn, dlg1* and *arm*

1657   showed enhanced necrotic patches compared with knockdown of *Cbp20*, while homozygous

1658   *Cbp20* RNAi and concomitant knockdown of *dlg1* showed increased necrotic patches

1659   compared with homozygous *Cbp20* RNAi. Furthermore, flies with knockdown of *dlg1* and

1660   *arm* both showed enhanced necrotic patches compared with individual knockdown of *dlg1* or

1661   *arm*. (**B**) Confocal images of pupal eyes (scale bar = 5 μm) stained with anti-DLG (top) and

1662   Phalloidin (bottom) illustrate enhanced defects in ommatidial and photoreceptor cell

1663   organization with concomitant *GMR-GAL4* RNAi knockdown of *Cbp20* and other fly

1664   homologs of 3q29 genes compared with *Cbp20* knockdown. (**C**) Larval eye discs (scale

1665   bar = 30 μm) stained with TUNEL show increases in apoptosis with pairwise knockdown of

1666   *Cbp20* and other fly homologs of 3q29 genes compared with recombined *Cbp20* knockdown

1667   crossed with control. (**D**) Box plot of TUNEL-positive cells in the larval eye discs of flies

1668   with pairwise knockdown of homologs of 3q29 genes (n = 9–13, *p < 0.05, two-tailed Mann–

1669   Whitney test with Benjamini-Hochberg correction). All boxplots indicate median (center

1670   line), 25th and 75th percentiles (bounds of box), and minimum and maximum (whiskers),

1671   with red dotted lines representing the control median. A list of full genotypes for fly crosses

1672   used in these experiments is provided in **S2 File**.

1673

1674

51

S10 Fig. Rescue of cellular phenotypes due to knockdown of fly homologs of 3q29 genes with overexpression of *Diap1*.

(**A**) Cellular phenotypes of flies with overexpression of *Diap1* and *Dronc*. Representative brightfield adult eye images (scale bar = 100 μm) and confocal images of larval eye discs (scale bar = 30 μm) stained with anti-dcp1 are shown for flies with *GMR-GAL4* overexpression of *Diap1* and *Dronc*, while confocal images of pupal eyes (scale bar = 5 μm) stained with anti-DLG are also shown for flies with overexpression of *Diap1*. While the overexpression of *Diap1* did not lead to any changes in the pupal or adult eye phenotype, overexpression of *Dronc* resulted in a large increase in apoptosis and depigmentation in the adult eye. (**B**) Box plot of *Flynotyper* distance ommatidial disorderliness (OD) scores for flies with concomitant *GMR-GAL4* RNAi knockdown of *Cbp20* or *dlg1* and overexpression of *Diap1* or *Dronc* is shown (n = 8–9, *p < 0.05, two-tailed Mann–Whitney test with Benjamini-Hochberg correction). (**C**) Box plot of *Flynotyper* angle OD scores for flies with knockdown of *Cbp20* or *dlg1* and overexpression of *Diap1* or *Dronc* is shown (n = 8–9, *p < 0.05, two-tailed Mann–Whitney test with Benjamini-Hochberg correction). The distance and angle OD scores, component subscores derived from *Flynotyper* [53], mirror the trends observed in the overall phenotypic scores (**Figure 6B**). (**D**) Box plot of adult eye area in flies with knockdown of *Cbp20* or *dlg1* and overexpression of *Diap1* or *Dronc* is shown (n = 8–9, *p < 0.05, two-tailed Mann–Whitney test with Benjamini-Hochberg correction). (**E**) Confocal images of pupal eyes (scale bar = 5 μm) stained with Phalloidin illustrate the rescue of photoreceptor cell organization defects due to knockdown of *Cbp20* or *dlg1* upon overexpression of *Diap1*. (**F**) Larval eye discs (scale bar = 30 μm) stained with TUNEL show rescue of apoptosis phenotypes observed in flies with knockdown of *Cbp20* or *dlg1* and overexpression of *Diap1*, as well as enhanced apoptosis with overexpression of *Dronc*. (**G**) Box plot of TUNEL-positive cells in the larval eye discs of flies with knockdown of *Cbp20* or *dlg1* and overexpression of *Diap1* or *Dronc* is shown (n = 7–10, *p < 0.05, two-tailed Mann–Whitney test with Benjamini-Hochberg correction). All boxplots indicate median (center line), 25th and 75th percentiles (bounds of box), and minimum and maximum (whiskers), with red dotted lines representing the control median. A list of full genotypes for fly crosses used in these experiments is provided in **S2 File**.

S11 Fig. Phenotypic scores for interactions between homologs of 3q29 genes and known neurodevelopmental genes in the adult fly eye.

(**A-D**) Box plots of phenotypic scores for concomitant *GMR-GAL4* RNAi knockdown of fly

52

1709 homologs of 3q29 genes and neurodevelopmental genes, compared with recombined lines for

1710 individual homologs of 3q29 genes crossed with controls, are shown (n = 2–10, *p < 0.05,

1711 two-tailed Mann–Whitney test with Benjamini-Hochberg correction). All boxplots indicate

1712 median (center line), 25th and 75th percentiles (bounds of box), and minimum and maximum

1713 (whiskers), with red dotted lines representing the control median. A list of full genotypes for

1714 fly crosses used in these experiments is provided in **S2 File**.

1715

1716 **S12 Fig. Quantification of 3q29 morpholino knockdown and apoptosis marker levels in**

1717 ***X. laevis* models.**

1718 (**A**) Electrophoretic gels show decreased expression of homologs of 3q29 genes due to

1719 morpholino (MO) knockdown at various concentrations in *X. laevis* embryos. Three

1720 replicates (uninjected and two MO concentrations) were performed for each morpholino, and

1721 band intensities were compared with expression of *ODC1* controls taken from the same

1722 cDNA samples and run on gels processed in parallel. (**B**) Quantification of expression for

1723 homologs of 3q29 genes at different MO concentrations, as measured by band intensity ratio

1724 to *ODC1* controls (n=3 replicates, *p<0.05, two-tailed Welch's T-test with Benjamini-

1725 Hochberg correction). (**C**) Full images of western blots for quantification of cleaved caspase-

1726 3 levels in *X. laevis* embryos with MO knockdown of homologs of 3q29 genes. Two replicate

1727 experiments were performed, and the intensity of bands at 19kD and 17kD (green arrows),

1728 corresponding with cleaved caspase-3, were normalized to those for the β-actin loading

1729 controls. Embryos injected with control MO, uninjected embryos, and embryos treated with

1730 30% EtOH as a positive control were included with the embryos injected with 3q29 MOs.

1731

1732 **S13 Fig. Eye phenotypes observed with knockdown of homologs of 3q29 genes in *X.***

1733 ***laevis* models.**

1734 (**A**) Representative eye images of stage 42 *X. laevis* tadpoles with MO knockdown of

1735 homologs of 3q29 genes (scale bar = 500 μm) show defects in eye size and morphology

1736 compared with the control (top). These defects were rescued with co-injection and

1737 overexpression of mRNA for homologs of 3q29 genes, as well as overexpression of the

1738 apoptosis inhibitor *xiap* for *ncbp2* (bottom). (**B**) Box plot of eye area in *X. laevis* models with

1739 knockdown of homologs of 3q29 genes, normalized to controls, is shown (n = 48–71,

1740 *p < 0.05, two-tailed Welch's T-test with Benjamini-Hochberg correction). Models with

1741 *ncbp2* knockdown and *xiap* overexpression showed an increased eye size compared with

1742 *ncbp2* knockdown. (**C**) Box plot of eye area in *X. laevis* models with knockdown of

1743 homologs of 3q29 genes and overexpression of mRNA for homologs of 3q29 genes,

1744 normalized to controls, is shown (n = 56–63, *p < 0.05, two-tailed Welch's T-test with

1745 Benjamini-Hochberg correction). All boxplots indicate median (center line), 25th and 75th

1746 percentiles (bounds of box), and minimum and maximum (whiskers), with red dotted lines

1747 representing the control median. The data shown for the eye area experiments represent

1748 pooled results of three experimental batches, and were normalized to the respective controls

1749 from each batch.

1750

1751 **S14 Fig. Replication of *Drosophila* experimental results for individual and pairwise**

1752 **knockdown of homologs of 3q29 genes.**

1753 (**A**) Replication dataset for climbing ability of select homologs of 3q29 genes over ten days.

1754 We replicated the defects in climbing ability observed with pan-neuronal RNAi knockdown

1755 of *Cbp20* and *dlg1*, while climbing defects in flies with knockdown of *Fsn* flies were not

1756 replicated in the second experimental batch and were therefore excluded from the main

1757 dataset (**Fig. 2B**). Data represented show mean ± standard deviation of 7-10 independent

1758 groups of 10 flies for each homolog. (**B**) Replication dataset for climbing ability of pairwise

1759 knockdown of homologs of 3q29 genes over ten days. We replicated the defects in climbing

1760 ability observed with pan-neuronal RNAi knockdown of *Cbp20/dlg1* and *Cbp20/Fsn*

1761 compared with recombined *Cbp20* knockdown crossed with control (**Fig. 3F**). Data

1762 represented show mean ± standard deviation of 5 independent groups of 10 flies for each

1763 homolog. (**C**) Replication dataset for adult eye area in flies with *GMR-GAL4* RNAi

1764 knockdown of homologs of 3q29 genes (n = 10-14, *p < 0.05, two-tailed Mann–Whitney test

1765 with Benjamini-Hochberg correction). We replicated the decreased eye sizes in flies with

1766 knockdown of *Cbp20* and *CG8888*, while flies with knockdown of *dlg1* showed a non-

1767 significant (p=0.154) increase in eye size (**Fig. 2D**). (**D**) Confocal images for replication

1768 dataset larval eye discs (scale bar = 30 µm) stained with anti-pH3 (top) and TUNEL (bottom)

1769 illustrate cellular defects posterior to the morphogenetic furrow (white box) upon knockdown

1770 of select fly homologs of 3q29 genes (**Fig. 2E**). (**E**) Replication dataset for pH3-positive cells

1771 in larval eye discs of flies with knockdown of homologs of 3q29 genes (n = 9-10, two-tailed

1772 Mann–Whitney test with Benjamini-Hochberg correction). As in the main dataset (**Fig. 2F**),

1773 we observed no significant changes in cell proliferation for flies with knockdown of *Cbp20*

1774 and *dlg1*. (**F**) Replication dataset for TUNEL-positive cells in larval eye discs of flies with

1775 knockdown of homologs of 3q29 genes (n = 6-8, *p < 0.05, two-tailed Mann–Whitney test

1776 with Benjamini-Hochberg correction). We replicated the increased apoptosis phenotypes

1777 observed with knockdown of *Cbp20* and *dlg1* (**S4 Fig.**). All boxplots indicate median (center

1778 line), 25th and 75th percentiles (bounds of box), and minimum and maximum (whiskers),

1779 with red dotted lines representing the control median. A list of full genotypes for fly crosses

1780 used in these experiments is provided in **S2 File**.

1781

1782 **S1 Table. *Drosophila* homologs of human 3q29 genes and expression of *Drosophila***

1783 **homologs during development.**

1784 DIOPT version 7.1 [100] and reciprocal BLAST were used to identify fly homologs of genes

1785 within the 3q29 region; six genes did not have fly homologs. Expression levels of fly

1786 homologs of 3q29 genes were assessed using high-throughput expression data from FlyAtlas

1787 Anatomy microarray expression data [104] and modENCODE Anatomy RNA-Seq data [105]

1788 from FlyBase.

1789

1790 **S2 Table. qPCR primers and expression values for RNAi knockdown of fly homologs of**

1791 **3q29 genes.**

1792 *Elav-GAL4* flies were crossed with RNAi lines of fly homologs of 3q29 genes at 25°C, and 3-

1793 4 day old adult *Drosophila* heads were used to quantify the level of expression compared

1794 with *Elav-GAL4* controls. *Elav-GAL4;;UAS-Dicer2* flies crossed with *CG5359* flies showed

1795 overexpression of *tiptop* [103] and were therefore excluded from further experiments. A list

1796 of full genotypes for fly crosses used in these experiments is provided in **S2 File**, and

1797 statistics for these data are provided in **S5 File**.

1798

1799 **S3 Table. Comparison of animal model phenotypes with knockdown or knockout of**

1800 **homologs of 3q29 genes.**

1801 Blue shaded boxes indicate previously identified phenotypes for individual homologs of 3q29

1802 genes, while "X" marks indicate recapitulated and novel phenotypes identified in our study.

1803 Gray-shaded boxes indicate that a homolog was not present in the model organism. Fly

1804 phenotypes were obtained from FlyBase [122], *X. laevis* phenotypes were obtained from

1805 Xenbase [120], and mouse knockout model phenotypes were obtained from the Mouse

1806 Genome Informatics database [123].

1807

1808 **S4 Table. Summary of scoring for phenotypic severity of axon targeting defects upon**

1809 **individual and pairwise knockdown of homologs of 3q29 genes.**

1810 Individual larval eye disc images were assigned mild, moderate or severe scores based on the

55

1811 severity of axon projection loss observed in each eye disc (see Methods). We found that the

1812 mild to moderate defects observed with knockdown of *Cbp20* were enhanced with

1813 concomitant knockdown of *dlg1* or *Fsn*, while *Diap1* overexpression partially rescued the

1814 defects observed with knockdown of *Cbp20* or *dlg1*. A list of full genotypes for fly crosses

1815 used in these experiments is provided in **S2 File**.

1816

1817 **S5 Table. Comparison of eye phenotypic scores for homologs of 3q29 genes and**

1818 **neurodevelopmental genes.**

1819 Table comparing *Flynotyper* scores for flies with *GMR-GAL4;UAS-Dicer2* RNAi knockdown

1820 of homologs of 3q29 genes (shaded in grey) with previously published scores for flies with

1821 *GMR-GAL4;UAS-Dicer2* RNAi knockdown of homologs of candidate neurodevelopmental

1822 genes [53].

1823

1824 **S6 Table. Analysis of defects in ommatidial cells with *GMR-GAL4* RNAi knockdown of**

1825 **fly homologs of 3q29 genes.**

1826 The number of "+" symbols displayed in the table indicate the severity of the observed

1827 cellular defects. Note that n=4-16 pupal eye preparations were assessed for each RNAi line

1828 tested. A list of full genotypes for fly crosses used in these experiments is provided in **S2**

1829 **File**.

1830

1831 **S7 Table. Screening for pairwise interactions among fly homologs of 3q29 genes.**

1832 "All interactions" indicates the number of pairwise crosses where at least one second-hit

1833 RNAi or mutant line showed enhancement of the single-hit phenotype, while "Validated"

1834 indicates the number of interactions which have two or more crosses with a second-hit RNAi

1835 or mutant line (if available) showing the same result. "Reciprocal cross" indicates the number

1836 of interactions with concordant results across pairs of reciprocal cross (i.e. *Cbp20*/*dlg1* vs.

1837 *dlg1*/*Cbp20*). These totals include crosses with the mutant line *Tsf2^{KG01571}*, as eye-specific

1838 RNAi knockdown of *Tsf2* was lethal, as well as flies heterozygous for *dlg1* RNAi and

1839 homozygous for *Cbp20* RNAi. Crosses with other RNAi or mutant lines for the same

1840 homolog (shaded in grey) are included as validation lines tested but were not counted as

1841 interactions. A list of full genotypes for fly crosses used in these experiments is provided in

1842 **S2 File**.

1843

1844 **S8 Table. Analysis of defects in ommatidial cells with pairwise *GMR-GAL4* RNAi**

1845 **knockdown of fly homologs of 3q29 genes.**

1846 The number of "+" symbols displayed in the table indicate the severity of the observed

1847 cellular defects. Note that n=4-16 pupal eye preparations were assessed for each interaction

1848 cross tested. A list of full genotypes for fly crosses used in these experiments is provided in

1849 **S2 File**.

1850

1851 **S9 Table. Screening for interactions between fly homologs of 3q29 genes and other**

1852 **known neurodevelopmental genes.**

1853 "All interactions" indicates the number of crosses where at least one second-hit RNAi line

1854 showed enhancement of the single-hit phenotype, while "Validated interactions" indicates the

1855 number of interactions which have two or more crosses with a second-hit RNAi or mutant

1856 line (if available) showing the same result. Results from two distinct fly homologs of

1857 *CHRNA7* that were crossed with homologs of 3q29 genes, *nAChRα6* and *nAChRα7*, were

1858 combined for the final number of interactions. Shaded interactions indicate pairwise crosses

1859 where the phenotypes observed with knockdown of the homolog for the neurodevelopmental

1860 gene by itself were suppressed with concomitant knockdown of homologs for 3q29 genes.

1861 The neurodevelopmental genes are annotated for cell cycle/apoptosis function (Gene

1862 Ontology terms GO:0007049 and GO:0006915) and association with microcephaly disorders

1863 [65]. A list of full genotypes for fly crosses used in these experiments is provided in **S2 File**.

1864

1865 **S10 Table. Developmental phenotypes observed in mouse models of the 3q29 deletion**

1866 **and individual homologs of 3q29 genes.**

1867 Comparison of mice with heterozygous deletion of the syntenic 3q29 region [14,15] with

1868 heterozygous knockout mouse models for *Dlg1* [14] and *Pak2* [72]. Blue shaded boxes

1869 indicate phenotypes observed in the knockout models, while gray-shaded boxes indicate a

1870 phenotype that was not tested in the knockout model. Neither *Dlg1*^{+/-} nor *Pak2*^{+/-} knockout

1871 mice recapitulate the body and brain weight, spatial learning and memory, or acoustic startle

1872 defects observed in the deletion mouse models.

1873

1874 **S11 Table. Summary of apoptosis function enrichment among candidate**

1875 **neurodevelopmental genes.**

1876 This table shows the number of candidate autism, intellectual disability and schizophrenia

1877 genes annotated for apoptosis function. The minimum, mean and maximum numbers of

57

1878   apoptosis genes in 100,000 simulated sets of candidate genes are shown, along with the

1879   percentiles and empirical p-values of the observed overlap with apoptosis genes for each

1880   simulation.

1881

1882   **S12 Table. Morpholinos used for *X. laevis* experiments.**

1883

1884   **S13 Table. qPCR primers used for *X. laevis* experiments.**

1885

1886   **S1 File. Pathogenicity metrics, mutations in disease cohorts, and biological functions of**

1887   **3q29 genes.**

1888   3q29 genes with Residual Variation Intolerance Scores (RVIS) <20th percentile [124] or

1889   probability of Loss-of-function Intolerant (pLI) scores >0.9 [125] are considered to be

1890   potentially pathogenic in humans and are shaded in gray. Mutations within 3q29 genes

1891   identified in disease cohorts were curated from three databases: denovo-db v.1.6.1 [75],

1892   GeneBook database (http://atgu.mgh.harvard.edu/~spurcell/genebook/

1893   genebook.cgi), and SFARI Gene [77]. Molecular functions for 3q29 genes were derived from

1894   RefSeq, UniProtKB and Gene Ontology (GO) individual gene summaries [126–128], and

1895   GO-SLIM terms for human genes and fly homologs were curated from PantherDB [101].

1896   Annotations for cell cycle/apoptosis and neuronal function were derived from GO Biological

1897   Process annotations for each gene.

1898

1899   **S2 File. List of fly stocks and full genotypes for all crosses tested.**

1900   This file lists the stock lines, stock center, and genotypes for primary and validation lines for

1901   fly homologs of 3q29 genes as well as neurodevelopmental and apoptosis genes outside of

1902   the 3q29 region. Full genotypes for the generated recombined lines as well as all individual

1903   and pairwise crosses tested in the manuscript are also listed in the file. BDSC: Bloomington

1904   *Drosophila* Stock Center; VDRC: Vienna *Drosophila* Resource Centre.

1905

1906   **S3 File. Transcriptome analysis of flies with knockdown of homologs of 3q29 genes.**

1907   This file lists all differentially expressed genes from RNA sequencing of flies with *Elav-*

1908   *GAL4* RNAi knockdown of homologs of 3q29 genes, as defined by log-fold change >1 or < -

1909   1 and false discovery rate (FDR) <0.05 (Benjamini-Hochberg correction). Human homologs

1910   identified using DIOPT are included for each differentially-expressed fly gene. The file also

1911   includes enriched Gene Ontology (GO) terms (p<0.05, Fisher's Exact test with Benjamini-

58

Hochberg correction) for each set of differentially-expressed fly genes, as well as lists of GO

terms enriched among their corresponding human homologs.

S4 File. List of candidate neurodevelopmental genes with apoptosis function.

This file lists 525 candidate neurodevelopmental genes that are annotated for apoptosis GO

terms, including their membership within pathogenic CNV regions.

S5 File. Statistical analysis of experimental data.

This file shows all statistical information (sample size, mean/median/standard deviation of

datasets, Shapiro-Wilk test statistics for normality, controls used, test statistics, p-values,

confidence intervals, and Benjamini-Hochberg FDR corrections) for all data presented in the

main and supplemental figures. Statistical information for ANOVA tests includes factors,

degrees of freedom, test statistics, and post-hoc pairwise t-tests with Benjamini-Hochberg

correction.

S1 Video. Climbing ability of flies with knockdown of individual homologs of 3q29 genes.

This video shows the climbing ability of *Elav-GAL4* control, *Cbp20* and *dlg1* individual

RNAi knockdown flies at day 10 of the climbing ability experiments.

S2 Video. Climbing ability of flies with pairwise knockdowns of homologs of 3q29 genes.

This video shows the climbing ability of *Cbp20/dlg1* and *Cbp20/Fsn* pairwise *Elav-GAL4*

RNAi knockdown flies at day 10 of the climbing ability experiments.

Table 1. Summary of major experiments for knockdown of homologs of 3q29 genes show widespread cellular and neuronal defects.

Experiment		RNAi knockdown of *Drosophila* homologs of 3q29 genes						
Phenotype	Assay	Cbp20	dlg1	Cbp20/dlg1	Cbp20/Fsn	Cbp20/CG8888	Cbp20/Diap1	dlg1/Diap1
Adult eye morphology	Rough eye phenotype	Rough eye	Rough eye	Enhanced rough eye	Enhanced rough eye	Enhanced rough eye	Rescue	Rescue
	Necrotic patches	None (Present in homozygous KD)	None	Yes (more severe in homozygous KD)	Yes	None	None	None
	Eye area	Decreased area	Increased area	NA	NA	NA	Rescue	Rescue
Neuronal phenotypes	Climbing ability	Climbing defects	Climbing defects	Enhanced climbing defects	Enhanced climbing defects	NA	NA	NA
	Axonal targeting	Axon targeting defects	Axon targeting defects	Enhanced targeting defects	Enhanced targeting defects	NA	Rescue	Rescue
Cell organization (pupal eye)	DLG staining	Cellular defects	Cellular defects	Enhanced cellular defects	Enhanced cellular defects	Enhanced cellular defects	Rescue	Rescue
	Phalloidin staining	Loss of photoreceptors	Loss of photoreceptors	No change	Enhanced photoreceptor loss	Enhanced photoreceptor loss	Rescue	Rescue
Cell cycle (larval eye disc)	pH3 staining	No change	No change	No change	No change	Decreased proliferation	NA	NA
	BrdU staining	No change	Increased proliferation	NA	NA	NA	NA	NA
Apoptosis (larval eye disc)	dcp1 staining	Increased apoptosis	Increased apoptosis	Increased apoptosis	Increased apoptosis	Increased apoptosis	Rescue	Rescue
	TUNEL assay	Increased apoptosis	Increased apoptosis	Increased apoptosis	Increased apoptosis	Increased apoptosis	Rescue	Rescue
Cellular phenotypes (larval wing disc)	pH3 staining	Decreased proliferation	Increased proliferation	NA	NA	NA	NA	NA
	dcp1 staining	Increased apoptosis	Increased apoptosis	NA	NA	NA	NA	NA
RNA sequencing (adult heads)	Differential gene expression	Synaptic transmission, metabolism	Synaptic transmission, ion transport	Cellular respiration, protein folding	Cell cycle, response to stimulus	NA	NA	NA

Experiment		Morpholino knockdown of *X. laevis* homologs of 3q29 genes						
Phenotype	Assay	ncbp2	fbxo45	pak2	ncbp2/fbxo45	ncbp2/pak2	ncbp2/xiap	fbxo45/xiap
Craniofacial morphology	Eye area	Decreased area	Decreased area	Decreased area	NA	NA	Rescue	NA
	Midbrain area	Decreased area	Decreased area	Decreased area	No change	No change	Rescue	NA
	Forebrain area	Decreased area	Decreased area	Decreased area	Decreased area	No change	Rescue	NA
Apoptosis	Cleaved caspase-3 levels	Increased caspase-3	Increased caspase-3	NA	Increased caspase-3	NA	Rescue	Rescue

Fig. 1

Tested *Drosophila* homologs

Tested *X. laevis* homologs

Human genes: ZDHHC19, OSTalpha, PCYT1A, TCTEX1D2, TM4SF19, UBXN7, TFRC, SMCO1, RNF168, WDR53, FBXO45, LRRC33, CEP19, PIGX, PAK2, SENP5, NCBP2, PIGZ, MFI2, DLG1, BDH1

Fly homologs: app, CG6836, Pcyt2, CG8892, CG5543, Fsn, PIG-X, Pak, Ulp1, Cbp20, PIG-Z, Tsf2, dlg1, CG8888

Drosophila single-hit models

Tissue-specific *GAL4* × *UAS-RNAi*

Drosophila two-hit models

GMR-GAL4 UAS-RNAi A × *UAS-RNAi* B

Global phenotype screening

Genes:
Ubiquitous: Larval lethality, Pupal lethality, Wing defects
Eye-specific: Small eyes, Large eyes, Rough eyes
Neuronal: Larval lethality, Pupal lethality, Climbing defect
Wing-specific: Lethality, Ectopic veins, Wrinkled wings, Discoloration

Pairwise interaction screening

161 pairwise crosses tested between 3q29 homologs

153 pairwise crosses tested with other neurodevelopmental genes

Neuronal phenotypes

Climbing ability   *Axonal targeting* (anti-chaoptin)

Cellular phenotypes

Adult eye morphology (Necrotic patches)   *Cellular organization* (DLG, Phalloidin)

Apoptosis and cell cycle mechanisms

Cell proliferation (DAPI, pH3)   *Apoptosis* (dcp1)   *Phenotype rescue with apoptosis inhibition (Diap1)* (DLG)   *Transcriptome analysis* (Gene Ontology terms)

Validation in *X. laevis* models

GFP+morpholino (2- or 4-cell stage)

Abnormal eye morphology   *Rescue with apoptosis inhibition (xiap)*

GFP+morpholino (2-cell stage)

Abnormal brain morphology (Tubulin, Uninjected, morpholino)   *Rescue with apoptosis inhibition (xiap)* (Uninjected, morpholino+ xiap OE)

Fig. 2

Fig. 3

A

Pairwise interactions for homologs of 3q29 genes

Single-hit RNAi lines (y-axis): $app^{KK108227}$, $Cbp20^{KK109448}$, $CG6836^{KK112485}$, $CG8888^{GD3777}$, $dlg1^{GD4689}$, $Fsn^{GD11383}$, $Pak^{KK101874}$, $PIG\text{-}X^{KK109747}$, $PIG\text{-}Z^{KK107404}$

Second-hit RNAi lines (x-axis): $app^{KK108227}$, $Cbp20^{KK109448}$, $CG6836^{KK112485}$, $CG8888^{GD3777}$, $dlg1^{GD4689}$, $Fsn^{GD11383}$, $Pak^{KK101874}$, $PIG\text{-}X^{KK109747}$, $PIG\text{-}Z^{KK107404}$

Score change legend: −5 to 25

B

Pairwise interactions of $Cbp20$ ($NCBP2$)

Phenotypic score (y-axis). Fly RNAi lines (x-axis): $Cbp20^{KK109448}/Control$, $Cbp20^{KK109448}/CG8888^{GD3777}$, $Cbp20^{KK109448}/dlg1^{GD4689}$, $Cbp20^{KK109448}/Fsn^{GD11383}$, $Cbp20^{KK109448}/Tsf2^{KK101571}$, $Cbp20^{KK109448}/CG6836^{KK112485}$, $Cbp20^{KK109448}/Pak^{KK101874}$, $Cbp20^{KK109448}/PIG\text{-}X^{KK110819}$, $Cbp20^{KK109448}/PIG\text{-}X^{KK109747}$, $Cbp20^{KK109448}/PIG\text{-}Z^{KK107404}$, $Cbp20^{KK109448}/Ulp1^{GD7581}$, $Cbp20^{KK109448}/CG8892^{GD14061}$, $Cbp20^{KK109448}/CG5543^{KK109031}$, $Cbp20^{KK109448}/app^{KK108227}$

C

Pairwise interactions of $dlg1$ ($DLG1$)

Phenotypic score (y-axis). Fly RNAi lines (x-axis): $dlg1^{GD4689}/Control$, $dlg1^{GD4689}/CG8888^{GD3777}$, $dlg1^{GD4689}/Fsn^{GD11383}$, $dlg1^{GD4689}/Tsf2^{KK101571}$, $dlg1^{GD4689}/Cbp20^{KK109448}$, $dlg1^{GD4689}/CG6836^{KK112485}$, $dlg1^{GD4689}/Pak^{KK101874}$, $dlg1^{GD4689}/Pcyt2^{KK110819}$, $dlg1^{GD4689}/PIG\text{-}X^{KK109747}$, $dlg1^{GD4689}/PIG\text{-}Z^{KK107404}$, $dlg1^{GD4689}/PIG\text{-}Z^{GD7581}$, $dlg1^{GD4689}/Ulp1^{GD7581}$, $dlg1^{GD4689}/CG8892^{GD14061}$, $dlg1^{GD4689}/CG5543^{KK109031}$, $dlg1^{GD4689}/app^{KK108227}$

D

Rough eye phenotypes of pairwise interactions

$Cbp20^{KK109448}/Fsn^{GD11383}$ — Enh. $Cbp20^{KK109448}/CG8888^{GD3777}$ — Enh. $Cbp20^{KK109448}/PIG\text{-}Z^{KK107404}$ — Enh.

$CG8888^{GD3777}/Fsn^{GD11383}$ — Enh. $PIG\text{-}Z^{KK107404}/Fsn^{GD11383}$ — Enh. $PIG\text{-}Z^{KK107404}/Cbp20^{KK109448}$ — Enh.

E

Axon targeting defects

$GMR\text{-}GAL4$ — anti-chaoptin; eye disc, optic stalk, lamina, medulla, R7-R8 projections. $Cbp20^{KK109448}$. $Cbp20^{KK109448}/dlg1^{GD4689}$ — Enh. $Cbp20^{KK109448}/Fsn^{GD11383}$ — Enh.

F

Climbing ability

Climbing ability (%) vs Experiment day. Fly RNAi lines: $Cbp20^{KK109448}/Control$, $Cbp20^{KK109448}/dlg1^{GD4689}$, $Cbp20^{KK109448}/Fsn^{GD11383}$
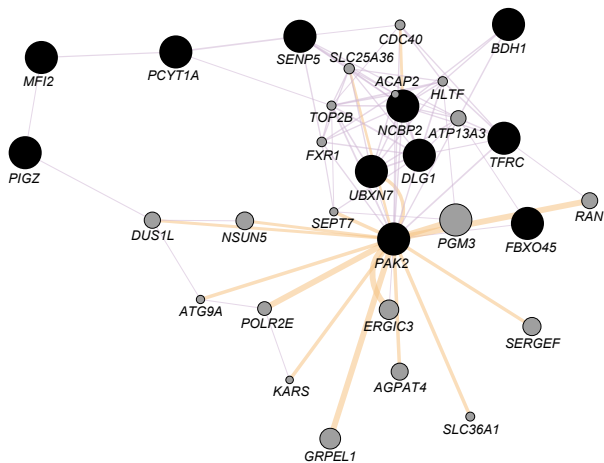
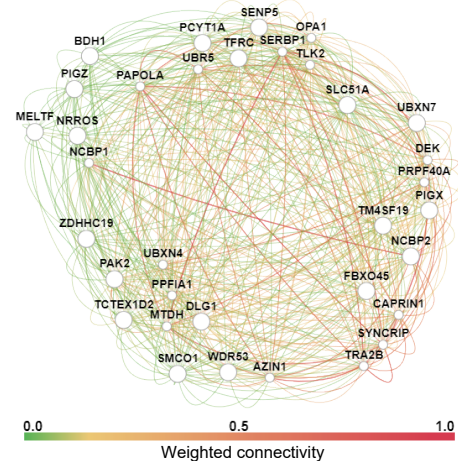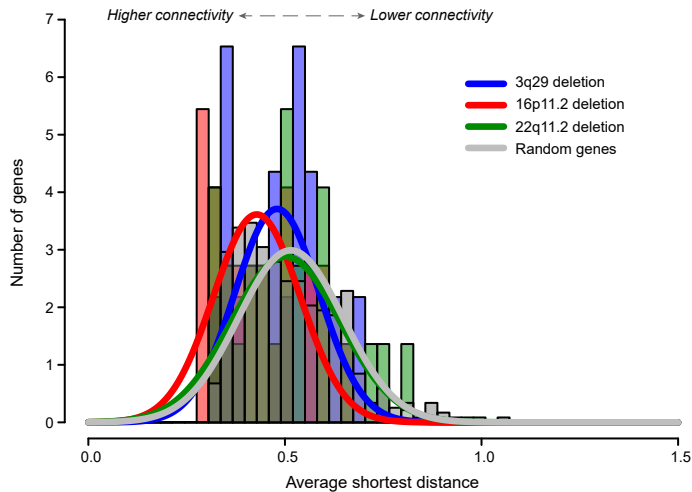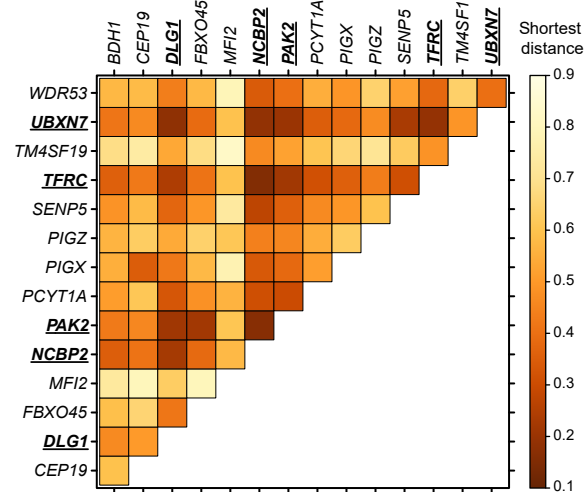# Fig. 4

A Human gene interaction network of 3q29 genes (GeneMania)

B Human gene interaction network of 3q29 genes (GIANT)

Weighted connectivity

C Average connectivity of CNV genes in human brain-specific network

Higher connectivity ← – – – → *Lower connectivity*

Number of genes

Average shortest distance

- 3q29 deletion
- 16p11.2 deletion
- 22q11.2 deletion
- Random genes

D Connectivity of 3q29 genes in human brain-specific network

Shortest distance

Fig. 5

A

Necrotic patches in the adult eye

Cbp20^{KK109448}/ Control

Cbp20^{KK109448}/ dlg1^{GD4689}

Necrotic patches

Enh.
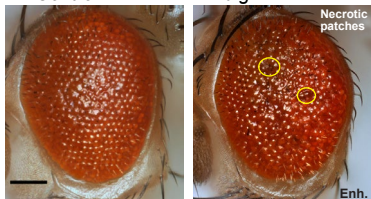
Homozyg. Cbp20^{KK109448}

Homozyg. Cbp20^{KK109448}/ Heterozyg. dlg1^{GD4689}

Enh.
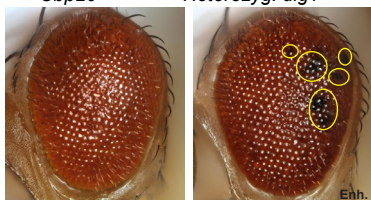
B

Cellular organization defects

Cbp20^{KK109448}

Cbp20^{KK109448}/ CG8888^{GD3777}

DLG
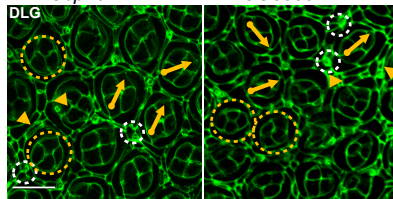
Cbp20^{KK109448}/ dlg1^{GD4689}

Cbp20^{KK109448}/ Fsn^{GD11383}
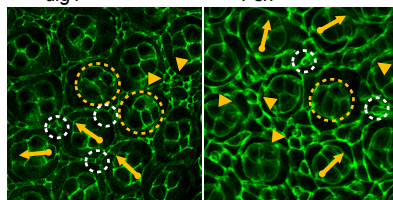
C

Photoreceptor cell defects

Cbp20^{KK109448}

Cbp20^{KK109448}/ CG8888^{GD3777}

Phalloidin
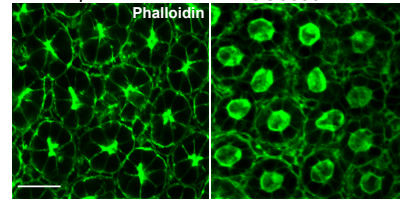
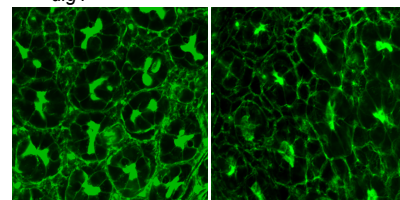*Cbp20^{KK109448}/ dlg1^{GD4689}*

Cbp20^{KK109448}/ Fsn^{GD11383}

D

Cellular phenotypes of pairwise knockdowns in the larval eye disc

Cbp20^{KK109448}/Control

Cbp20^{KK109448}/ CG8888^{GD3777}

Cbp20^{KK109448}/ dlg1^{GD4689}

Cbp20^{KK109448}/ Fsn^{GD11383}

Apoptosis — dcp1

Proliferation — pH3 DAPI

E

Apoptosis defects

dcp1 positive cells

1000
800
600
400
200

* * *

Cbp20^{KK109448}/Control
Cbp20^{KK109448}/CG8888^{GD3777}
Cbp20^{KK109448}/dlg1^{GD4689}
Cbp20^{KK109448}/Fsn^{GD11383}
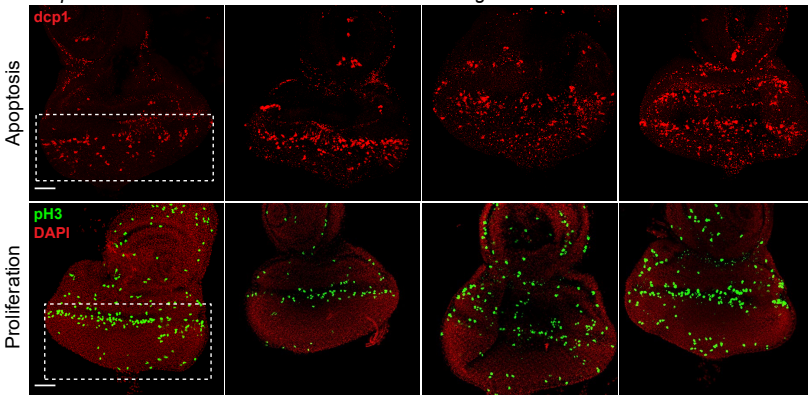
Fly RNAi lines
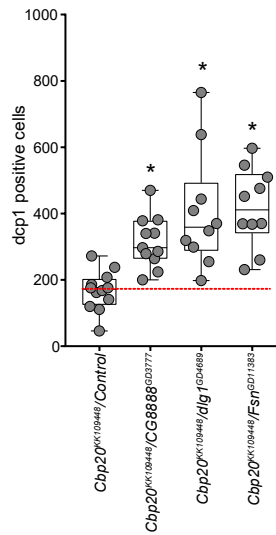
F

Cell proliferation defects

pH3 positive cells

600
400
200
0

* ns ns

Cbp20^{KK109448}/Control
Cbp20^{KK109448}/CG8888^{GD3777}
Cbp20^{KK109448}/dlg1^{GD4689}
Cbp20^{KK109448}/Fsn^{GD11383}

Fly RNAi lines

Fig. 6

A

Adult eye phenotypes with *Diap1/Dronc* overexpression

dlg1^GD4689

dlg1^GD4689/ Overexp Diap1

dlg1^GD4689/ Overexp Dronc — Rescue

Cbp20^KK109448

Cbp20^KK109448/ Overexp Diap1 — Rescue

Cbp20^KK109448/ Overexp Dronc — Necrotic patches, Enh.

B

Rough eye phenotypes

Phenotypic score vs Fly RNAi lines

C

Necrotic patches

Necrotic patch area (µm²) vs Fly RNAi lines

D

Rescue of cell organization defects

DLG

dlg1^GD4689

dlg1^GD4689/ Overexp Diap1

Cbp20^KK109448

Cbp20^KK109448/ Overexp Diap1

E

Apoptosis phenotypes in the larval eye disc

dcp1

dlg1^GD4689

dlg1^GD4689/ Overexp Diap1

dlg1^GD4689/ Overexp Dronc — Rescue

Cbp20^KK109448

Cbp20^KK109448/ Overexp Diap1 — Rescue

Cbp20^KK109448/ Overexp Dronc — Enh.

F

Quantification of apoptotic cells

dcp1 positive cells vs Fly RNAi lines

G

Rescue of axon targeting defects

anti-chaoptin

Cbp20^KK109448

Cbp20^KK109448/ Overexp Diap1 — Supp.

dlg1^GD4689

dlg1^GD4689/ Overexp Diap1 — Supp.

Fig. 7

A

Pairwise interactions with homologs of neurodevelopmental genes

Second−hit RNAi lines (neurodevelopmental genes)

First-hit RNAi lines (3q29 homologs)

Score change

B

Rough eye phenotypes of pairwise interactions

Fig. 8

A

Injection at 2-cell stage

Brain morphology defects in *X. laevis* tadpoles

D

Western blot for apoptosis marker

B

Forebrain area defects

C

Midbrain area defects

E

Quantification of western blot bands

Fig. 9

A

Phenotypic severity →

Enhanced phenotypes
with Cbp20 interaction

Interactions of other
3q29 homologs

Drosophila homologs of 3q29 genes

app | CG6836 | Pcyt2 | CG8892 | CG5543 | Fsn | PIG-X | Pak | Ulp1 | Cbp20 | PIG-Z | dlg1 | Tsf2 | CG8888

B

● 3q29 genes

Cell cycle

NCBP2

Apoptosis

Synaptic transmission

Neurodevelopmental
phenotypes